RAMAN SPECTROSCOPIC EVIDENCE FOR SIDE-ON BINDING OF

PEROXIDE ION TO FERRIC-EDTA

Salman Ahmad
B.S., Reed College, 1985

A thesis submitted to the faculty
of the Oregon Graduate Center
in partial fulfillment of the
requirements for the degree
Master of Science
in
Chemistry

September, 1988

The thesis "Raman Spectroscopic Evidence for Side-On Binding of

Peroxide Ion to Ferric-EDTA" by Salman Ahmad has been examined and

approved by the following Examination Committee:

Thomas M. Loehr, Thesis Research Advisor
Professor

Joann Sanders-Loehr, Thesis Research Advisor
Professor

Ninian J. Blackburn
Associate Professor

TABLE OF CONTENTS

ABSTRACT

Raman Spectroscopic Evidence for Side-On Binding of
Peroxide to Ferric-EDTA

Salman Ahmad, M.S.
Oregon Graduate Center, 1988

Supervising Professors: Thomas M. Loehr and Joann Sanders-Loehr

Resonance Raman spectra of the complex of Fe^{III}-ethylenediamine-
tetraacetate with hydrogen peroxide have been obtained in the region of
the peroxidic O-O stretching vibration that occurs at 815 cm^{-1} in
frozen solution. When the complex was prepared from nearly neat,
mixed-isotope hydrogen peroxide, $H_2{}^{16}O^{18}O$, a single O-O vibration was
observed at 794 cm^{-1}. This observation establishes that the two oxygen
atoms of the bound peroxide are equivalent and that the peroxide is
ligated in an η^2 side-on configuration in this mononuclear complex.
The absence of any shift in ν(O-O) when the complex was prepared in D_2O
solvent provides further support for the $Fe\overset{O}{\underset{O}{<}|}$ geometry and rules out
the alternative η^1 end-on Fe-OOH configuration. In contrast, ν(O-O) of
free hydrogen peroxide in the frozen state occurs at 877 cm^{-1} in H_2O
and at 879 cm^{-1} in D_2O. The 2-cm^{-1} upshift in D_2O is similar to that
observed previously with oxyhemerythrin and appears to be
characteristic of a hydrogen-bonded or protonated peroxide species.

iv

CHAPTER I

THE STRUCTURE AND ELECTRONIC SPECTRA OF

TRANSITION METAL-DIOXYGEN COMPLEXES

Introduction

The point of departure for a discussion of the molecular structure and electronic spectra of transition metal-dioxygen complexes is a consideration of the electronic structure of O_2 in its ground state and a comparison of some fundamental physical properties of ground state O_2 with those of other dioxygen species.

Owing to its electrophilic nature, O_2 is an unusual ligand when it binds to transition metals. Generally, electron transfer from the metal orbitals to the higher-lying orbitals of O_2 takes place, (partially) reducing it, and conferring upon it the electronic structure, physical properties and, to an extent, chemical reactivity of superoxide, $O_2^-\cdot$, and peroxide, O_2^{2-}. In many reactions, O_2 may bind to transition metal complexes as a superoxo or peroxo species. However, the precise assignment of an oxidation state to O_2 and to the metal is sometimes ambiguous and speculative.

In this chapter, a classification scheme for dioxygen complexes first introduced by Vaska will be described. The two fundamental structural types of this scheme have O_2 bound as side-on and end-on species. The electronic structure of these two types of metal complexes will be described and molecular orbital (MO) diagrams corresponding to them will be constructed. Finally the electronic structure of a side-on O_2 complex, Fe^{III}-ethylenediaminetetraacetate-peroxide, $Fe^{III}(edta)O_2^{2-}$, will be discussed. MO diagrams will be

presented and the two known charge transfer transitions will be assigned and their selection rules described.

Electronic Structure of Ground-State O_2.
A Comparison with Other O_2 Species

The electronic configuration of dioxygen as a neutral molecule is KK $\sigma_{2s}^2 \; \sigma_{2s}^{*2} \; \pi_{2p}^4 \; \pi_{2p}^{*1} \; \pi_{2p}^{*1}$ and, hence, it exhibits a triplet ground state, $^3\Sigma_g^-$. The spin multiplicity arises from the electrons in the HOMO π_g^* orbitals. The reactions of O_2 in its ground state with organic molecules are generally slow,[1] because most organic molecules have a singlet ground state. Singlet-triplet reactions, which involve a change of spin, are thermally forbidden. If an organic molecule is first excited to a triplet state, then its reaction with ground state oxygen may proceed without a change of spin. However, the product molecule then formed is in an excited triplet state which, in most cases, is unstable. If O_2 is photochemically excited to its first excited state, $^1\Delta_g$, then the reaction can proceed at a useful rate.

Other more reactive (or "activated") forms of O_2 may be obtained either by the ionization of one of the π_g^* electrons or by the systematic addition of electrons to the HOMO π_g^* levels. This is shown schematically in Figure 1. It is clear that in going from $O_2^{+\cdot}$ to O_2^{2-}, the order of the O–O bond decreases systematically. The evidence for this comes mainly from the variation in the O–O distance, R(O–O), and in the O–O stretching frequency, ν(O–O). Representative values are shown in Table I, where some patterns are clearly discernible. As the order of the O–O bond, and hence the force constant associated with the

O–O stretching vibration, decreases, so does the value of $\nu(O\text{–}O)$. The frequency regions characteristic of neutral O_2, $O_2^{-\cdot}$, and O_2^{2-} are distinct. The bond distance shows the opposite trend and increases systematically in the series from $O_2^{+\cdot}$ to O_2^{2-}. Again, the bond length values for the various dioxygen species are in fairly distinct ranges. As expected, the energy of the O–O bond decreases with a decrease in bond order.

A Structural Classification of Transition Metal–O_2 Complexes.
The Scheme of Vaska

Many transition metals form stable complexes with dioxygen. These may arise from the reaction of a neutral metal atom or metal ion with molecular oxygen, superoxide or peroxide. The bonding in these complexes arises from the interaction of the HOMO π* orbitals of the O_2 with metal d–orbitals of suitable symmetry and energy. Depending upon the most energetically favorable interaction possible, several different types of structures are observed. The most useful classification of these is the one proposed by Vaska.[2] In this scheme metal–O_2 complexes fall into four basic types which are given in Table II. The nomenclature describing these structural types uses the "hapto" designation, η, where structures are classified according to the number of O atoms bound to a metal, hence, η^1 and η^2. The basis for designating the structural types as I and II rests with the identification of the bound O_2 as a superoxo or peroxo species, respectively. Type I complexes generally have an R(O–O) of ~1.3 Å and a $\nu(O\text{–}O)$ at ~1120 cm^{-1}, whereas type II complexes exhibit a longer

4

R(O–O) of ~1.45 Å and a correspondingly lower ν(O–O) between ~750–900 cm^{-1}. A third classification, a or b, refers to the number of metal ions, 1 (mononuclear) or 2 (dinuclear), respectively. In this thesis, only mononuclear complexes, type a, are considered having one O_2 coordinated to one metal atom. The two most generally observed orientations, the bent end-on configuration and the side-on configuration, are shown in Table II.

The classification scheme of Table II is based upon the range in which ν(O–O) and R(O–O) are observed for a given metal–O_2 complex. However, there are a number of transition M–O_2 complexes for which such values are intermediate between those for $O_2^{-\cdot}$ and O_2^{2-} (Table I). For these, the assignment of type I or II is ambiguous.

Electronic Structures of Type Ia and IIa M–O_2 Complexes

The 3d-orbital energies in the first transition series rise from 7 eV for Sc to 17 eV for Zn. The energy of the HOMO π^* orbitals in $^3\Sigma_g^-$ O_2 is about 12 eV.[3] Thus, in bond formation between transition metals and O_2 the strongest interaction takes place between the π^* orbitals on the ligand and the outer d-orbitals on the metal of the appropriate symmetry. This interaction is primarily responsible for the observed geometry and the charge-transfer (CT) electronic transitions in these complexes.

Significant interaction also takes place between the σ(2p) and π orbitals on the dioxygen (which lie at about 15 eV in neutral ground state dioxygen[3]) and the metal d-orbitals. However, the former are fully occupied bonding orbitals that can only behave as donors and O_2

is an electrophilic ligand. This is unusual in that most ligands in transition metal complexes are basic. Net dislocation of electron density from the metal to the O_2 may, therefore, only take place in the interaction of the metal d-orbitals with the $\pi*$ orbitals on the dioxygen.[4] Other empty orbitals on O_2 are so far removed in energy from the metal d-orbitals that no significant interaction takes place.

It is intended to present here a qualitative discussion of the bonding in transition metal complexes of η^1- and η^2-type structures, corresponding to complexes of type Ia and IIa, respectively. The bonding scheme described is between an ML_n fragment and O_2. Here M is the transition metal atom (or ion) and L are the other ligands in the metal-O_2 complex. The following set of assumptions are made in this discussion:

1. In the interaction of an O_2 molecule with an ML_n fragment, the core and M-L bonding levels of the ML_n entity do not make a significant contribution to the bonding.

2. The 4s and 4p orbitals on the metal in the first transition series may make a significant contribution to the bonding. However, for reasons of symmetry and energy, their main interactions are with the fully occupied $\pi(2p)$ and $\sigma(2p)$ orbitals on O_2. These σ-like interactions do not differentiate between η^1 and η^2 structures.

3. The $\sigma(2s)$ and $\sigma*(2s)$ orbitals on O_2 lie at 25 and 40 ev, respectively.[3] They are thus too stabilized to be available for significant interactions with metal valence orbitals.

4. The $\sigma*(2p)$ orbital on O_2 has negative energy.[3] It is too destabilized to interact significantly with any occupied metal-based

orbitals.

As a consequence of the four assumptions given above[4] we are left with the following orbitals with which to construct an MO description of the bonding between an O_2 ligand and an ML_n fragment:

    a. The $\sigma(2p)$, π, and $\pi*$ and orbitals on O_2.

    b. The metal 3d-orbitals: d_{xy}, d_{xz}, d_{yz}, $d_{x^2-y^2}$, d_{z^2}.

Extended Hückel calculations[4,5] have been used to obtain the relative magnitudes of the overlaps between the metal and ligand based orbitals. The bonding overlaps between the d-orbitals on M and the $\pi*$ orbitals on O_2 for η^1 (Ia) and η^2 (IIa) structures are given in Figure 2. The Cartesian axes are chosen such that, for the η^1 geometry, the z-axis is coincident with the M-O bond and the x-axis is in the M-O-O plane. For the η^2 geometry, the z-axis contains the metal atom and bisects the O-O bond while the x-axis is parallel to the O-O bond.

Other than the non-zero overlaps indicated in Figure 2, the significant overlaps of metal d-orbitals with O_2 orbitals are the following[4]:

1. For an η^1 geometry d_{z^2} has significant interaction with the O_2 $\sigma(2p)$ orbital. This is strong for a linear M-O-O geometry but decreases on going to a bent structure (M-O-O angle <180°). Since $\sigma(2p)$ is a filled donor orbital on an electrophilic ligand the main consequence of the interaction is to destabilize dz^2.

2. For an η^2 geometry d_{z^2} has significant interaction with both the $\sigma(2p)$ and π_z orbitals on the O_2. This is best represented by forming hybrid bonding and antibonding type orbitals from the $\sigma(2p)$ and π_z orbitals on O_2. Since the mixing of $\sigma(2p)$ and π_z is small, since

$\sigma(2p)$ is of a g symmetry while π_z is of u symmetry, the energy separation $\sigma(2p) + \pi_z$ and $\sigma(2p) - \pi_z$ is not large. However, $\sigma(2p) + \pi_z$ has appropriate symmetry to interact with d_z2 and cause destabilization of this orbital. This is illustrated in Figure 3A. The $\sigma(2p) + \pi_z$ orbital on the O_2 is a completely filled bonding orbital. Its separation in energy from d_z2 is considerable. For the Mn^{II}-porphyrin system, the d_z2 orbital occurs at 9.5 eV.[5] The $\sigma(2p) + \pi_z$ orbital is expected to be about 15 eV in energy.[4] The mixing of the d_z2 and $\sigma(2p) + \pi_z$ orbitals is therefore not expected to be large. The net effect of this interaction is to stabilize the $\sigma(2p) + \pi_z$ hybrid and destabilize d_z2. The effect of bonding $\sigma(2p)$ and π O_2 orbitals on the metal d-orbitals will be ignored in constructing the MOs.

3. For an η^2 geometry the d_{yz} orbital has a non-zero overlap with the π_y orbital on the O_2. This destabilizes the d_{yz} orbital, as illustrated in Figure 3B.

Now we can proceed to construct generalized MO diagrams for η^1 and η^2 type structures.[6] Since O_2 is an electrophilic ligand, no net dislocation of electron density is expected to take place from the bonding O_2 orbitals to the metal d-orbitals. We start with bonding and antibonding orbitals using the non-zero overlaps (Fig. 2) and then to fill in the total number of electrons in the d-orbitals of M and the interacting π^* orbitals of the O_2 entity.

Figure 4 shows a generalized MO diagram for an η^1 $M-O_2$ complex. The relative d-orbital energies are taken for a metalloporphyrin, MP, where the x- and y-axes lie along opposite pyrrole nitrogens.[5] The z-axis is coincident with the M-O bond and the xz-plane is the metal-O_2

plane. The strongly σ-bonding $d_{x^2-y^2}$ is the highest energy d-orbital

and d_{z^2} is destabilized by an axial ligand <u>trans</u> to the coordinated O_2.

The metal in the ML_n fragment has five d-electrons in the high-spin

state (e.g., Mn^{II}, Fe^{III}) and this configuration is retained in going

to ML_nO_2. The π^* orbitals on the dioxygen contribute 2 e^-s to make it

a 7-e^- system. It is notable that due to the weak interaction between

$\pi^*_{||}$ and d_{z^2} (Fig. 2A) the energy of the bonding σ-orbital is somewhat

higher than that of the bonding π-orbital. In this system the energy

of the (σ^*-like) orbital $d_{z^2}-\pi^*_{||}$ lies below that of $d_{x^2-y^2}$. Thus, on

going from ML_n to ML_nO_2, the $d_{x^2-y^2}$ orbital loses its unpaired e^-. Such

predictions made from high field NMR data may be confirmed by extended

Hückel calculations.[5,13]

Figure 5 shows a generalized MO diagram for an η^2 M-O_2 complex.

The d-orbital energies, as in Figure 4, are taken from a metallo-

porphyrin. The x- and y-axes are oriented as before, and the z-axis is

coincident with the M-O bond and bisects the O-O bond axis. The

configuration described by the MO diagram of Figure 5 has the O-O bond

axis parallel to the x-axis. The high-spin d^5 metal in ML_n retains

this configuration in ML_nO_2. The dioxygen HOMO π^*-orbitals contribute

two e^-s to make it a 7-e^- system. The strong σ-interaction between d_{xz}

and $\pi^*_{||}$ is indicated clearly. This causes the σ and σ^* orbitals to be

the most and least stable, respectively. Here the high energy $d_{x^2-y^2}$

lies below σ^* and retains its unpaired electron on going from ML_n to

ML_nO_2. Also indicated on this diagram is the energy of the antibonding

type orbitals formed by mixing the $\sigma(2p)$ and π orbitals of the O_2

entity (Fig. 3A). These are somewhat destabilized relative to the π

orbitals on the O_2 and should be close to the σ ($\pi^*_{||}$ + d_{xz}) orbital in energy. Their significance will be discussed later in the section on the electronic spectra of Fe^{III}edta.

In the formation of a M–O_2 complex the O_2 species may contribute two, three or four e^-s depending upon whether it is an O_2, $O_2^{-\cdot}$, or O_2^{2-} species. The generalized MOs (Figs. 4 and 5) then simply accommodate the correct total number of e^-s. If the complexing species is $O_2^{-\cdot}$ instead of neutral O_2, then the system has a total of 8 e^-s. These may be filled into the MOs (Fig. 4) to give species whose total spin varies from a possible minimum of S = 0 to a maximum of S = 3. The complexes may be distinguished from each other by magnetic moment measurements. However, the assignment of specific oxidation states to the M and the O_2 species is more difficult.

For instance, in the η^1 complex ML_nO_2 of Figure 4, if the bonding $\pi^*_\perp$ + d_{yz} and $\pi^*_\perp$ + d_{z^2} orbitals are considered to be mainly O_2 orbitals, then it is clear that one e^- has been completely or partially transferred from the metal d-orbitals to the O_2 π^* orbitals upon complex formation. The extent of such a transfer may be inferred from data from spectroscopic studies and MO calculations. The former include high field NMR, which may indicate whether a particular metal d-orbital is populated or vacant, and infrared and Raman vibrational spectroscopy from which a value of ν(O–O), and hence the type of O_2 species involved, may be obtained. Extended Hückel calculations give the relative energies of the metal d-orbitals and the O_2 π^* orbitals and the magnitude of the orbital overlaps. Thus the electron density in the various metal-type and ligand-type MOs may be inferred.

However, the assignment of specific oxidation states to the metal and to the O_2 ligand is often a matter of considerable ambiguity and speculation.

The energies of the metal d-orbitals in an ML_n fragment depend greatly upon the metal, its oxidation state and the nature of the ligands L. Hence, the energies of the MOs formed by the interaction of ML_n with O_2 will also depend upon these factors. Also important is the geometry of the ML_n fragment which will determine the relative energies of the metal d-orbitals. In addition, steric and hydrogen-bonding effects will determine the most facile arrangement for the binding of O_2. However, all other things taken to be equal, the large σ-interaction between $\pi^*_{||}$ and d_{xz} (Fig. 2B and 5) would tend to make η^2 complexes more stable than η^1 complexes. The overwhelming majority of $M-O_2$ complexes, for which the structures are known, exhibit the η^2 side-on binding of O_2.

The Structure of Fe^{III}edta in the Crystalline State

Figure 6 shows the core structure of Fe^{III}edta which is known from X-ray crystallography.[6] It is a seven-coordinate complex made up of the sexadentate edta and a water molecule. Five atoms in the inner coordination sphere of the iron are in an approximately pentagonal arrangement. The interior bond angles of this pentagon sum from 515-535°, vs. 540° for an ideal pentagon. A two-fold axis (the maximum allowable symmetry for this structure) which passes through the $Fe-OH_2$ bond, and the center of the C_1-C_2 (ethylene) bond. The C_2 symmetry is pretty well retained by the whole molecule and the greatest

distortions, which are observed within or near the inner coordination sphere, are not significant ($\leq 2°$). Likewise, the bond lengths which are required to be equal by the C_2 symmetry differ by <0.1 Å.

The average bond lengths of the $Fe^{III}(edta)H_2O$ structure are listed in Table III. The iron atom forms two short Fe-O bonds with the trans O_1 and O_2 atoms. With an O_1FeO_2 angle of 162.6°, the structure approximates a pentagonal bipyramid whose basal plane is formed by O_w, O_3, N_2, N_1, O_4. The metal forms two longer Fe-O bonds to O_3 and O_4, and the Fe-O_w bond is about the same length. The iron-nitrogen bonds are considerably longer, indicating that they contribute much less to the stability of the structure than the Fe-O bonds. The $Fe^{III}(edta)H_2O$ complex is very stable (log $K_f \simeq 25.1$). This is due to the strong interaction between the very basic, σ-donating "hard-base" ligands provided by the charged acetate oxygens and the very "acidic" high oxidation state metal.

The structure of the $Fe^{III}(edta)H_2O$ complex is unusual, and considerably different from the more typical "octahedral" structure displayed, e.g., by $Mn(edta)H_2O$.[7] In the latter structure, the four Mn-O bonds to the acetate oxygens are equal and in the same plane while the Mn-O_w bond is normal to it, as is the line passing from the Mn and bisecting the N-Mn-N angle made by the two equal Mn-N bonds. The surprising difference from $Fe(edta)H_2O$ is the length of the planar Mn-O bonds to the acetate oxygens which average 2.236 Å.[7] The $Mn(edta)H_2O$ is obviously the less strained "natural" orientation of the ligand atoms provided by edta and H_2O. The strain introduced by the unusual geometry of $Fe(edta)H_2O$ is compensated by the greater stability of the

shorter Fe-O bonds which average to 2.06 Å (Table III).

Lind et al.[6] suggest a possible contribution of covalent bonding between the σ-donor ligands of edta/H_2O and the empty $4sp^3$ orbital set on the iron atom. In this bonding scheme, the $4p_z$ orbital on the Fe^{3+} forms a σ interaction with the axial O_w. The hybrid orbital formed by the interaction of 4s and $4p_y$ orbitals interacts with O_1 and O_2. The remaining $4p_x$ orbital is then involved in a 2-e$^-$, 3-center bonding scheme with O_3 and O_4. It is the ~35° departure of the O_3-Fe-O_4 angle from linearity which weakens this type of bonding and causes the Fe-O_3 and Fe-O_4 bonds to be longer than Fe-O_1 and Fe-O_2. However, this type of interaction with the (high energy) $4sp^3$ set of orbitals is not the main source of the stabilization energy of the Fe^{III}(edta)H_2O complex which comes from the electrostatic interaction between the basic oxygen and nitrogen ligands and an acidic, trivalent metal ion.[8]

The Structure of Fe^{III}edta in Solution

The iron atom in the mononuclear complex formed by iron and edta in solution is known to be in the high-spin +3 state.[9] Thus it is likely that the strong interaction between the metal ion and the hard base type oxygen ligands from the acetate groups observed in the solid is maintained in solution. At high pH, the seven-coordinate geometry of Fe^{III}(edta)H_2O (Fig. 6) appears to be maintained in solution as indicated by the unusually high value of log K_f = 25 for this complex. The short Fe-O bonds would yield a high enthalpy of formation. Potentiometric studies indicate that a water molecule remains bound to Fe^{III}edta in solution, ionizing to Fe^{III}(edta)OH$^-$ with a pK_a of 7.8.[8]

However, at low solution pH, distortions of the molecule would be expected as a consequence of the relief of strain introduced by its crystal geometry. The configuration of the acetate O and ethylene N ligands in the seven-coordinate structure shown in Figure 6 suggests a mechanism of such a distortion by protonation of one of the acetate O atoms which form the long Fe—O bonds (O_3 or O_4). Assuming O_3 is the oxygen atom protonated, then a counterclockwise motion of the atoms O_4, N_1 and N_2 in the plane of the pentagon would yield the pseudo-octahedral, six-coordinate structure shown in Figure 7. The original short Fe—O_1 and Fe—O_2 bonds would be retained, and would be coplanar with the longer Fe—O_4 and Fe—N_2 bonds. The Fe—N_1 bond would become axial _trans_ to the water molecule.

The prerequisite to the formation of the pseudo-octahedral six-coordinate structure shown in Figure 7 is the protonation of O_3 or O_4. This is not likely to happen at high pH (the pK_a of acetic acid is 4.8). Thus in the formation of the $Fe^{III}(edta)O_2^{2-}$ complex which takes place at pH > 10 there can be little doubt that the seven-coordinate structure would be retained in solution. Bull et al. in studying the reduction of Fe^{III}edta by $O_2^{-}\cdot$ report an anomalous increase of the reaction rate below pH > 7.[8] They suggest that a more reactive form of Fe^{III}edta could be the predominant species below pH 7. This could be the pseudo-octahedral six-coordinate species shown in Figure 7 or some similar structure. The implications of this will be discussed later in the chapter on the reactivity of Fe^{III}edta.

The Assignment of the Electronic Spectrum of the

Fe^{III}(edta)peroxo Complex

The peroxo complex of Fe^{III}edta is formed by the reaction of H_2O_2

with Fe^{III}edta in aqueous solution of pH > 10 at 0°C.[9] It is

characterized by a purple color which is due to an electronic absorp-

tion at 520 nm (ε = 530 M^{-1} cm^{-1}). A second and much more intense

transition is at 287 nm (ε = 6100 M^{-1} cm^{-1}).[9,10] The physical

properties of the Fe^{III}(edta)$O_2{}^{2-}$ complex are well characterized. It

has a magnetic moment of 6.03-6.07 B.M. at pH > 10. This is character-

istic of Fe^{III} in the high-spin configuration.[9] Excitation within the

520-nm band gives the resonance Raman spectrum of the Fe^{III}(edta)$O_2{}^{2-}$

complex, which is characterized by the presence of ν(O–O) in the region

815-825 cm^{-1}.[10,11] This is in the correct range for the bound O_2

species to be classified as a peroxide. The resonance Raman

enhancement profile of ν(O–O), a plot of the intensity of a ν(O–O) vs.

the wavelength of the exciting radiation, approximately tracks the λ =

520-nm band.[10]

The λ = 520 nm transition has been assigned to an O_2 ligand-to-

metal-charge-transfer (LMCT) band.[9] The CT character of this band

(under some doubt due to its low absorptivity) is confirmed by its

responsiveness to the resonance Raman technique. The other band at 287

nm is undoubtedly from a CT transition.

A qualitative but descriptive MO electronic configuration diagram

for the Fe^{III}(edta)$O_2{}^{2-}$ complex will be constructed in this section.

It will be assumed that, at pH > 10, Fe^{III}edta maintains the same

structure as in the crystalline state.[7] The formation of the peroxide

complex by the reaction of Fe^{III}edta with H_2O_2 has been thoroughly studied.[8,11] Here it will be assumed that peroxide binds to Fe^{III}edta by the displacement of the axial H_2O, and that the stoichiometry of the $Fe^{III}(edta)O_2^{2-}$ complex is 1:1 in Fe^{III}edta and peroxide.[8,9]

The O_2^{2-} may bind to the Fe^{III}edta complex in an η^1 or η^2 manner. Vaska's classification scheme (Table I) of $M-O_2$ complexes suggests that the likely structure for a M-peroxo complex is η^2 (side-on). The proof that this is the configuration of the bound O_2 in $Fe^{III}(edta)O_2^{2-}$ comes from resonance Raman (rR) spectroscopy using mixed isotope $O^{16}-O^{18}$ dioxygen.[11] These experiments are presented and discussed in detail in Chapter II. Here it will be assumed that, in the $Fe^{III}(edta)O_2^{2-}$ complex, the O_2^{2-} is bound in an η^2 configuration.

The Cartesian coordinates[6] of the core atoms of the $Fe^{III}(edta)H_2O$ complex are displayed in a two-dimensional representation in Figure 8. The numbers are adjusted only slightly to give an idealized two-fold symmetry with the C_2-axis coincident with the z-axis. The iron atom lies at the origin, and the positive z-axis bisects the O-O bond. Any orientation of the O-O bond axis that is neither parallel to the x- nor the y-axis will give little or no overlap of the O_2 π^* orbitals with the d-orbitals of the metal. This interaction is primarily responsible for the stability of the $M-O_2$ bond.

The structure where the O_2^{2-} binds with its bond axis parallel to the x-axis is considered first. This is the same configuration as that of O_2 bound as shown in Figure 2B. The d_{xz} orbital on the metal has a strong σ-bonding interaction with $\pi^*_{||}$, the O_2 π^*-orbital in the $M-O_2$ plane. The O_2 π^*-orbital perpendicular to the $M-O_2$ plane has a weak δ

interaction with the d_{xy} orbital on the metal.

Before going on to construct the MO diagrams for the $Fe^{III}(edta)O_2^{2-}$ complex it is necessary to consider the effect of the ligand field (LF) of edta (provided by atoms O_1, O_2, O_3, O_4, N_1, N_2) on the energies of the 3d-orbitals. Although the absolute values of the energies of the 3d-orbitals are not known, comparison with other systems may give some idea of the magnitude of the splitting of the 3d-orbitals by the LF of edta. In the Mn^{II}-porphyrin system[5] (also a high-spin d^5 complex), the maximum energy separation in the d-orbital set is ~2 eV. The Mn^{II} ion is displaced out of the porphyrin plane by ~0.5 Å, creating long Mn-N bonds which average 2.184 Å. The Fe-O bonds in Fe^{III}edta average 2.056 Å and two of them (to O_1 and O_2) average only 1.97 Å. Moreover, the acetate oxygen are harder ligands than the pyrrole nitrogens, and, therefore, the interaction between the acetate oxygens and the Fe^{III} will be substantially greater than that between the pyrrole nitrogens and Mn^{II}. Hence, the maximum splitting of the d-orbitals in the Fe^{III}edta system is estimated to be ~3 eV.

The expected relative energies of the iron 3d-orbitals in the LF of edta for the approximately pentagonal bipyramidal structure are shown at the left of Figure 9 with a maximum splitting of ~3 eV. The relative energies of the d-orbitals are assigned on the strength of the following considerations:

1. The $d_{x^2-y^2}$ orbital has a large σ interaction with O_1 and O_2 (Fig. 8). The Fe-O bonds to these atoms are short, and atoms O_1 and O_2 are displaced only 8.9° from the y-axis (along the x-axis) and 7.4° from the y-axis (along the z-axis). In addition, the $d_{x^2-y^2}$ orbital

also has substantial interaction with O_3 and O_4 which lie at a displacement of 10.2° from the x-axis (along y) and 17.8° from the x-axis (along z). Thus, the $d_{x^2-y^2}$ orbital is at the highest energy.

2. The d_{xz} orbital has its main interaction with the σ-donor (sp^3 hybridized) orbital on each nitrogen, N_1 and N_2. Although the nitrogen lone-pair interactions are not as strong as those enumerated in 1, the lobes of the d_{xz} orbital are at a displacement of only 8° from the Fe-N bond axes.

3. The other 3d-orbitals of the iron have no significant interaction with the LF of edta, and may be regarded to be lowest in energy and nearly degenerate. The axial water molecule has been excluded from this LF.

The MO diagrams for $Fe^{III}(edta)O_2^{2-}$ are constructed in the same way as those of Figures 4 and 5. The orbital overlaps for an η^2 configuration are given in Figure 2B. The metal 3d-orbital-O_2 π*-orbital system has a total of 9 e^-s, and must be filled into the MOs with the stipulation that the resulting configuration have five unpaired e^-s.[9] This leaves the $π*_{||} + d_{xz}$ and $π*_\perp + d_{xy}$ levels fully occupied and all other levels singly occupied.

The MO diagram for O_2^{2-} bound in a side-on geometry to Fe^{III}edta, with the O-O bond parallel to the x-axis, is given in Figure 9. The only difference from the MO diagram of Figure 5 is that the σ*-orbital ($d_{xz} - π*_{||}$) is drawn lower in energy than the $d_{x^2-y^2}$ orbital. This is done to take into account the exceptionally strong interaction of the $d_{x^2-y^2}$ orbital with the acetate oxygens of edta. The energies of the d_{yz} and d_{z^2} orbitals are drawn somewhat destabilized relative to their

positions in Fe^{III}edta. This is because of the interaction of the

metal d_{z^2} orbital with the $\sigma(2p) + \pi_z$ orbital and of the metal d_{yz}

orbital with the π_y orbital (Fig. 3A, B). The energies of the $\sigma(2p)-\pi$

hybrid orbitals are also shown (Fig. 9), and it is expected to lie

close to the bonding $d_{xz} + \pi^*_{||}$ orbital.[5] The C_2 symmetry element of

Fe^{III}(edta)H_2O is preserved for the structure which has O_2^{2-} bound in

an η^2 configuration. The MOs in Figure 9 have been assigned as a_1 or

b_1 according to whether they are symmetric or antisymmetric with

respect to rotation.

Figure 10 shows the MO diagram for O_2 bound to Fe^{III}edta in an η^2

configuration with the O—O axis parallel to the y-axis. The only

difference from the results in Figure 9 is that now the strongly σ-

bonding d-orbital in the M–O_2 plane is d_{yz}. The δ-interaction between

$\pi^*_{\perp}$ and d_{xy} is still present.

The assignment of the 520–nm transition in the electronic

absorption spectrum of Fe^{III}(edta)O_2^{2-} is done on the strength of the

following considerations:

1.   The intensity of the 520-nm band is too strong ($\varepsilon = 530$ M^{-1}

cm^{-1}) for a pure d–d transition but weak for a CT band.

2.   Its responsiveness to the rR technique confirms its CT

character.

3.   In the rR spectrum, ν(O—O) is enhanced selectively over

ν(Fe–O_2) which, if present, is barely above the noise level.

4.   The rR intensity enhancement profile of ν(O—O) tracks the 520–

nm band but its maximum is at 545 nm. This is indicative of the

presence of an unresolved peak which is the "active component" in the

rR effect. Thus, it is actually the rR-active component of the 520-nm band of $Fe^{III}(edta)O_2^{2-}$ which can being assigned.

Transition metal-peroxo complexes with O_2 bound in an η^2 geometry exhibit a characteristic absorption band in the 750-400-nm range.[14] This is a weak transition ($\varepsilon = 100-1000\ M^{-1}\ cm^{-1}$) and often has a shoulder or additional peak close in energy to it. This band has been assigned to a $\pi^*_{\perp} \rightarrow$ metal LMCT band.[14] From Figure 9, this may be assigned as a $\delta(\pi^*_{\perp} + d_{xy}) \rightarrow d_{z^2}$, $\delta \rightarrow d_{yz}$ or $\delta^* \rightarrow d_{x^2-y^2}^*$ transition. The energy of the $\delta \rightarrow d_{x^2-y^2}$ transition is expected to be >520 nm.

Figure 11A shows the orientation of the electric dipole $\hat{\mu}$ of the transition $\delta(\pi^*_{\perp} + d_{xy}) \rightarrow d_{z^2}$. Because of its weak, δ-type inter-action with d_{xy}, $\pi^*_{\perp} + d_{xy}$ is mainly π^*-like in character (Fig. 2B), and lies along the line OL (Fig. 11A) parallel to the y-axis and normal to the $M-O_2$ (xz) plane. The d_{z^2} orbital lies along the z-axis.

The $\delta^*(\pi^*_{\perp} - d_{xy})$ orbital is mainly a d_{xy} orbital, so that a $\delta^* \rightarrow d_{x^2-y^2}$ transition is in the main a d-d transition which would probably not be responsive to rR enhancement. The direction of $\hat{\mu}$ will be from out of the xz-plane to into the xz-plane. Because the electric dipole from an out-of-plane to an in-plane orbital is small,[14] the $\delta \rightarrow d_{z^2}$ transition would be expected to be weak is the case for the 520-nm band.

However, $\hat{\mu}$ may be resolved in components $\hat{\mu}_{||}$, in the xz-plane, and $\hat{\mu}_{\perp}$, normal to the xz-plane. The normal component will not couple to charge displacement along either the O-O or the Fe-O bonds during a vibrational motion. However, $\hat{\mu}_{||}$ is able to couple with σ-electron density displacement along both the O-O and Fe-O bonds. Thus, one

would expect the resonance enhancement of both $\nu(O-O)$ and $\nu(Fe-O)$ in the rR spectrum of $Fe^{III}(edta)O_2^{2-}$. Experimentally only the enhancement of $\nu(O-O)$ is observed (Chapter II).[10,11]

Figure 11B is drawn on the same principles as Figure 11A, and illustrates the orientation of the dipole, $\hat{\mu}$, of the $\delta(\pi^*_\perp + d_{xy}) \rightarrow d_{x^2-y^2}$ transition. $\hat{\mu}$ may be resolved into two components: $\hat{\mu}_{||}$, in the xz-plane and $\hat{\mu}_\perp$, normal to the xz-plane. However, note that $\hat{\mu}$ itself lies outside the xz-plane. It is clear that $\hat{\mu}_{||}$ may couple to the displacement of σ-electron density along the O-O and Fe-O bonds. This is inconsistent with the selective enhancement of $\nu(O-O)$ in the resonance Raman spectrum of $Fe^{III}(edta)O_2^{2-}$.

Figure 12 illustrates the orientation of the electric dipole $\hat{\mu}$ for the electronic transition $\delta(d_{xy} + \pi^*_\perp) \rightarrow d_{yz}$ (Fig. 9). Since the orientation of the dipole $\hat{\mu}$ is parallel to the xz-plane, it would not couple with the change in polarizability of σ-electron density in either the O-O or Fe-O bonds vibrations whose bonds lie in the xz-plane. However, $\hat{\mu}$ would couple strongly with the electron density polarization of the O-O π and π^* orbitals, during a vibration. Thus the selective enhancement of $\nu(O-O)$ over $\nu(Fe-O)$ in the resonance Raman spectrum may be accounted for.

The polarizability of the π and π^* electron density of the O-O bond would change by a small amount during an Fe-O vibration. This is due to the outward motion of the oxygen atoms during an $Fe-O_2$ symmetric stretching vibration. However, the R(O-O) (on which the polarizability of π and π^* electron density of O_2 depends) would only increase by a small amount. In the $\nu(O-O)$ vibration, the change in R(O-O) is large

and so the polarizability of the π and π^* electron clouds will change significantly. It is also to be noted that both $\nu(O\text{-}O)$ and the $Fe\text{-}O_2$ symmetric stretching vibrations have A_2 symmetry in the C-2 point group of the η^2 structure of O_2 binding to Fe^{III}edta assumed for this discussion.

On the strength of the aforementioned considerations, the 520-nm transition in Figure 9 (O-O axis parallel to the x-axis) is assigned as the $\delta(d_{xy} + \pi^*_\perp) \rightarrow d_{yz}$ transition. This would yield an excited state of B_1 symmetry and would be x,y-polarized. The same transition ($\lambda = 520$ nm) is assigned to the $\delta(\pi^*_\perp + d_{xy}) \rightarrow d_{xz}$ transition for the case where the O-O bond axis is parallel to y (Fig. 10). There, too, it would yield a B_1 excited state and would be x,y-polarized.

The high energy ($\lambda = 287$ nm) transition is an intense band ($\varepsilon = 6100$ M^{-1} cm^{-1}),[8,9] and would, therefore, be expected to be an LMCT transition between two orbitals in the same plane.[14] From these considerations this transition is assigned as either the $\sigma(\pi^*_{||} + d_{xz}) \rightarrow \sigma^*(\pi^*_{||} - d_{xz})$ or $\sigma(2p) - \pi_{||} \rightarrow \sigma^*$ transition (Fig. 5A) for the structure for which the MO diagram of Figure 9 has been constructed. The former transition yields an A_1 excited state and is z-polarized. The latter transition has a B_1 excited state and is (x,y) polarized.

It is to be noted that both the 520-nm and 287 nm transitions have been assigned as occurring from a bonding, dioxygen-like, orbital to either an antibonding metal-like orbital or to a pure metal orbital. Therefore, as assigned, these are LMCT transitions. This is in agreement with the assignment of the 520-nm transition in the literature.[9]
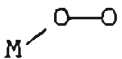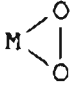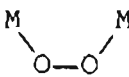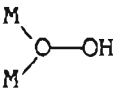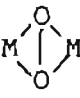
REFERENCES

(1) Gubelmann, M. H.; Williams, A. F. Struct. Bonding (Berlin) 1983, 55, 1.

(2) Vaska, L. Acc. Chem. Res. 1976, 9, 175.

(3) Ballhausen, C. J.; Gray, H. B. Molecular Orbital Theory; W. A. Benjamin, New York, 1964, p. 120.

(4) Hoffmann, R.; Chen, M. L.; Thorn, D. Inorg. Chem. 1977, 16, 503.

(5) Van Atta, R. B.; Strouse, C. E.; Hanson, L. K.; Valentine, J. S. J. Am. Chem. Soc. 1987, 109, 1425.

(6) Lind, M. D.; Hamor, M. J.; Hoard, J. L. Inorg. Chem. 1964, 3, 34.

(7) Richards, S. Pederson, B.; Silverton, J. V.; Hoard, J. L. Inorg. Chem. 1964, 3, 27.

(8) Bull, C.; McClune, G. J.; Fee, J. A. J. Am. Chem. Soc. 1983, 105, 5290.

(9) Walling, C.; Kurz, M.; Schugar, H. J. Inorg. Chem. 1970, 9, 931.

(10) Hester, R. E.; Nour, E. M. J. Raman Spectrosc. 1981, 11, 35.

(11) Ahmad, S.; McCallum, J. D.; Shiemke, A. K.; Appelman, E. H.; Loehr, T. M.; Sanders-Loehr, J. S. Inorg. Chem. 1988, 27, 2230.

(12) Orhanovic, M.; Wilkins, R. G. Croat. Chem. Acta 1967, 39, 149.

(13) Hanson, L. K.; Hoffman, B. M. J. Am. Chem. Soc. 1980, 102, 4602.

(14) Lever, A. B. P.; Gray, H. B. Acc. Chem. Res. 1978, 11, 348.

Table I. Variation of the O–O distance and ν(O–O) in the various known O_2 species.[a]

Species	Bond Order	Compound	O–O distance (Å)	ν(O–O) (cm^{-1})	Bond energy (kJ mol^{-1})
$O_2^{+\cdot}$	2.5	O_2AsF6	1.123	1858	625
O_2 (S=3)	2.0	O_2	1.207	1555	490
O_2 (S=1)	2.0	O_2	1.216	1484	396
$O_2^{-\cdot}$	1.5	HO_2			
$O_2^{-\cdot}$	1.5	KO_2	1.32–1.35	1146	
$O_2^{-\cdot}$	1.5	$O_2^{-\cdot}$ (g)	1.34		
O_2^{2-}	1.0	H_2O_2 (s)	1.453	877	
O_2^{2-}	1.0	Na_2O_2	1.50	794	204

[a] Data taken from reference 1.

Table II. Experimentally Observed Modes of Dioxygen Binding in Metal
Complexes [a]

Structural type	Vaska classification	dioxygen classification	dioxygen coordination
M—O—O (M)	Type Ia	superoxo	η^1
M(O,O) peroxo ring	Type IIa	peroxo	η^2
M···O—O···M bridge	Type Ib	superoxo	$\eta^1 : \eta^1$
	Type IIb	peroxo	$\eta^1 : \eta^1$
M,M—O—OH	Type IIb	peroxo	η^1
M(O,O)M bridge	Type ?b	?	$\eta^2 : \eta^2$

[a] Data taken from reference 1 and 2.

Table III. Structural parameters of $Fe^{III}(edta)H_2O$ [a]

Bond type	Average bond length (Å)
$Fe-O_1$	1.97
$Fe-O_2$	1.97
$Fe-O_3$	2.12
$Fe-O_4$	2.12
$Fe-O_w$	2.11
$Fe-N$	2.33

[a] Data from reference 6.

σ_u^* (2p)
LUMO

π_g^* (2p)
HOMO

$O_2^{+\cdot}$
(S=2)

O_2
(S=1)

O_2
(S=3)
ground state

$O_2^{-\cdot}$
(S=2)

O_2^{2-}
(S=1)
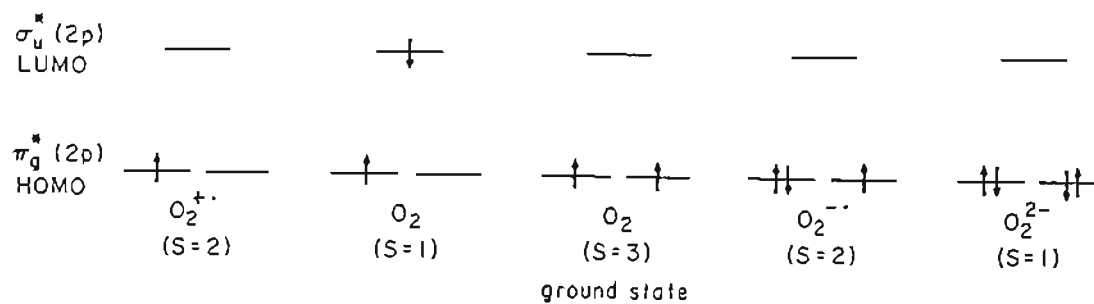
Figure 1. Electronic occupancy of the highest—occupied molecular orbitals (HOMOs) of several dioxygen species. The energies of the orbitals of the HOMO and LUMO orbitals are not the same from one species to another. Only a single excited state for neutral O_2 is shown, although many arrangements are possible.

$\pi^*_{||} + dz^2$
(σ-interaction)

$\pi^*_{\perp} + dyz$
(π-interaction)

A

$\pi^*_{||} + dxz$
(σ-interaction)

$\pi^*_{\perp} + dxy$
(δ interaction)

B
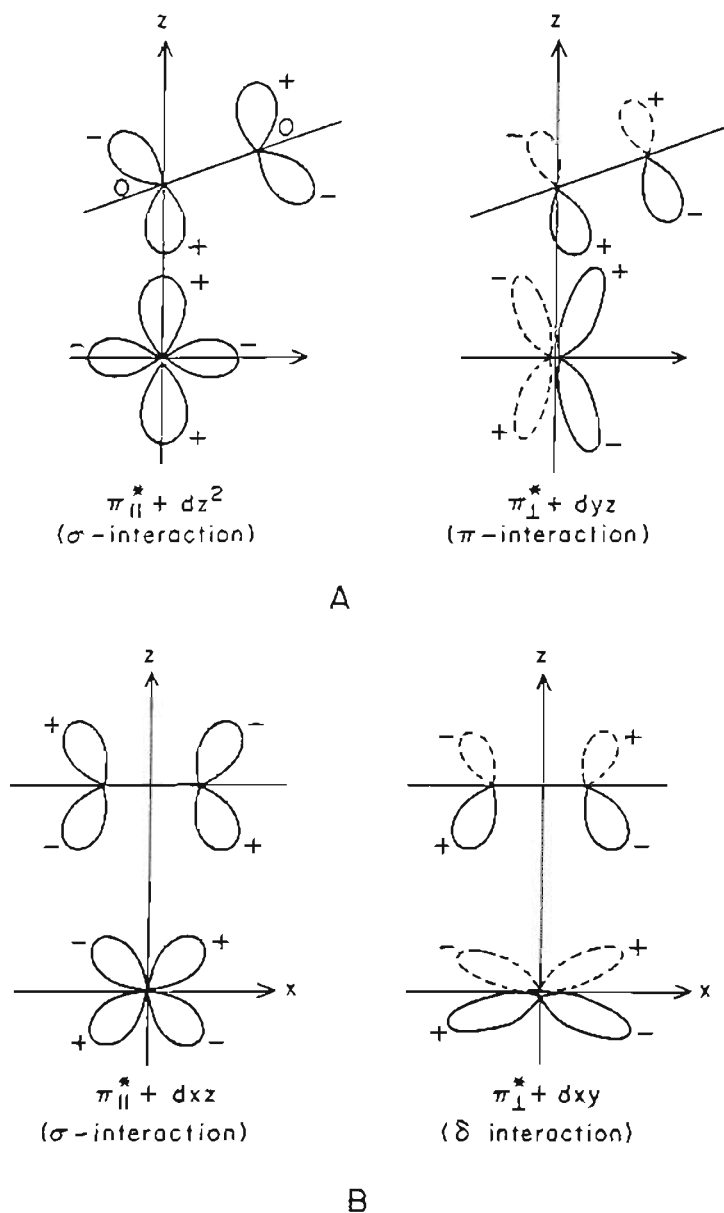
Figure 2. Diagrams illustrating the overlaps between the π^* orbitals on O_2 and various d-orbitals of a transition metal. $\pi^*_{||}$ and $\pi^*_{\perp}$ refer to the π^* orbitals in the $M-O_2$ plane and normal to the $M-O_2$ plane, respectively. A. For an η^1 (Class Ia) end-on coordinated O_2 in a mononuclear complex. B. For an η^2 (Class IIa) side-on coordinated O_2 in a mononuclear complex.
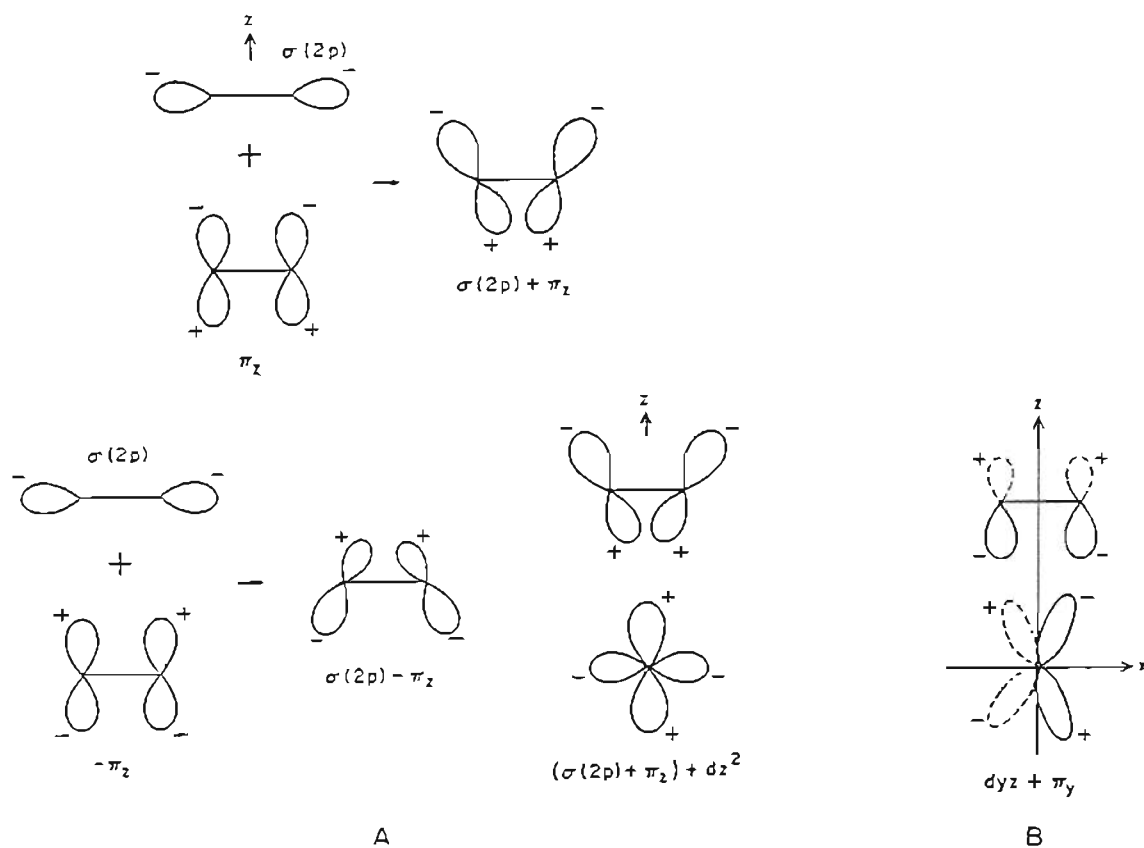
Figure 3. A. Formation of hybrid orbitals among dioxygen MOs that are bonding and antibonding, respectively, with the metal d_z2 orbital for an η^2 M-O_2 complex. Only the bonding interaction with d_z2 is shown. B. Non-zero overlap leading to a net σ-interaction between the dioxygen π_y and metal d_{xy} orbitals for an η^2 M-O_2 complex.
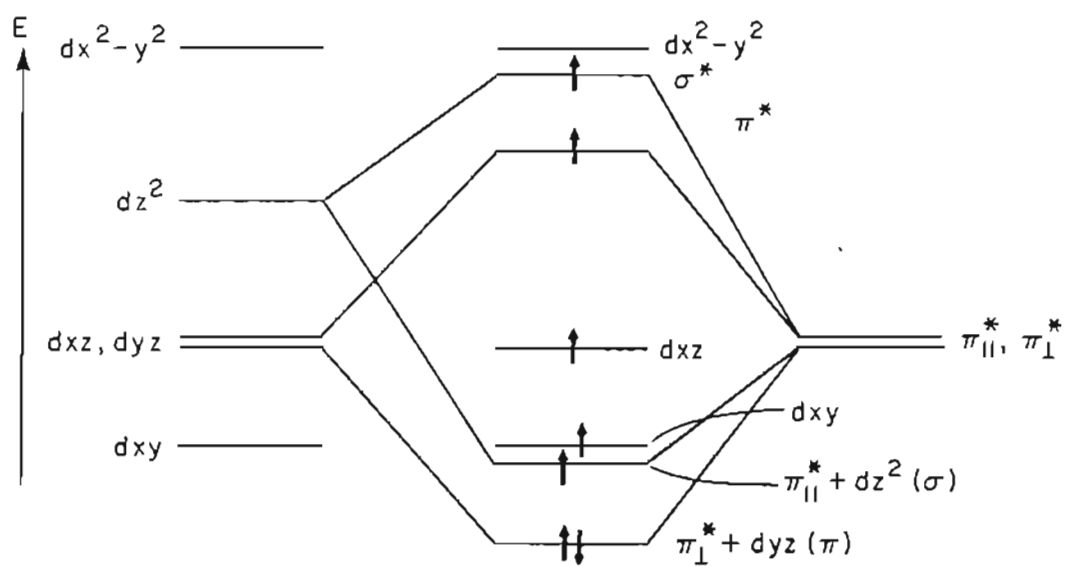
Figure 4. Qualitative MO for an η^1 M–O_2 complex. See discussion on pages 7 and 8.
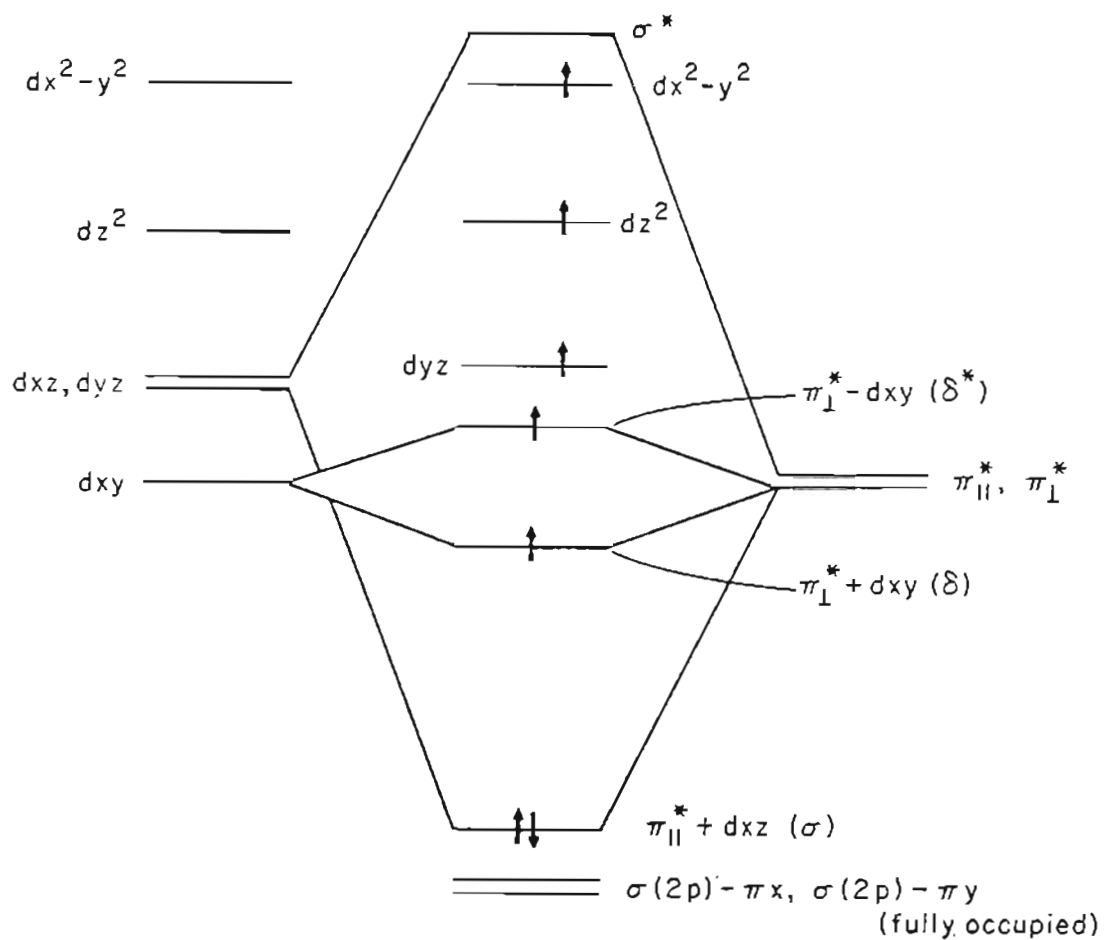
Figure 5. Qualitative MO for an η^2 M—O_2 complex. See discussion on pages 8 and 9.

31
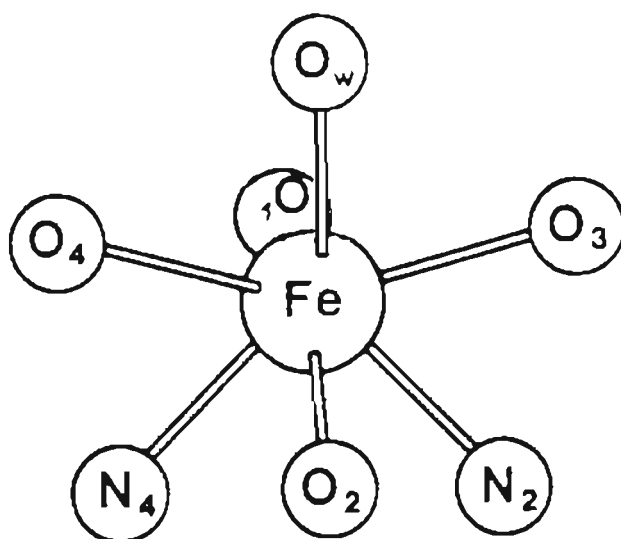
Figure 6. The coordination environment of the iron in $Fe^{III}(edta)H_2O$ showing the approximate pentagonal bipyramidal arrangement of six edta ligands and a water molecule around the seven-coordinate iron.[6]
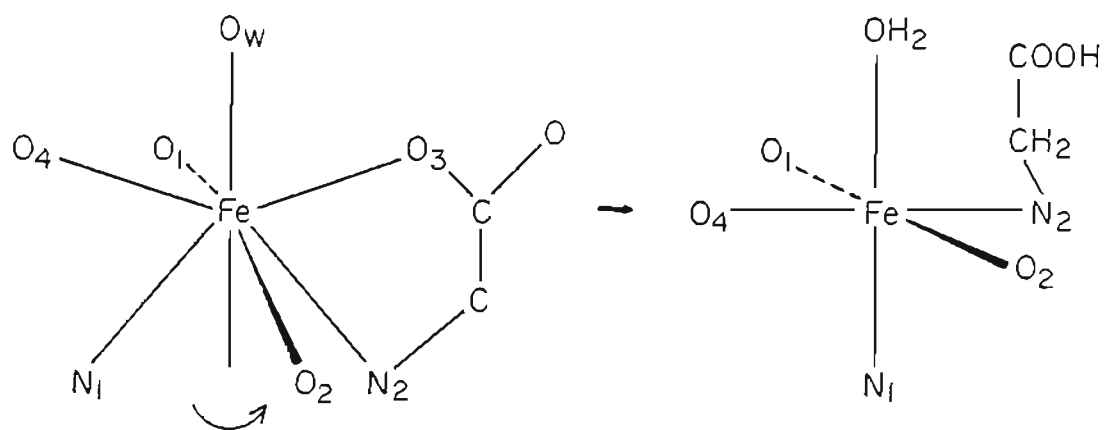
Figure 7. Proposed "mechanism" for a structural rearrangement of $Fe^{III}(edta)H_2O$ from the 7-coordinate pentagonal bipyramid to a 6-coordinate octahedron upon protonation of one of the acetate arms (the specific case for protonation of O3 is illustrated). See discussion on page 13.
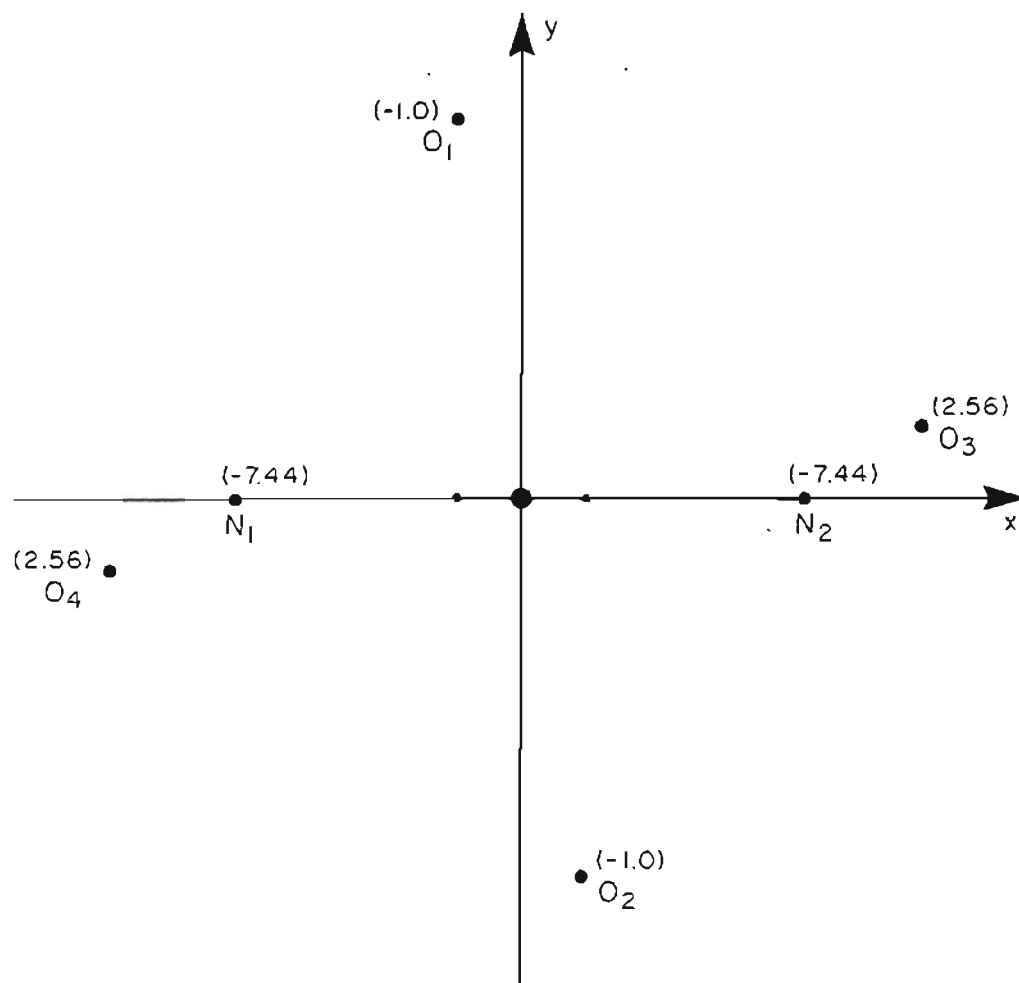
Figure 8. The Cartesian coordinates of the atoms in the inner coordination sphere around the iron atom in $Fe^{III}(edta)H_2O$ projected onto a reference plane containing the central iron atom. The numbers are adjusted slightly to give an idealized C_2 symmetry. The x-and y-axes are as indicated while the positive z-axis passes through the oxygen of the water molecule situated above the origin. The values of the z-coordinate are in parentheses. From Reference 6.
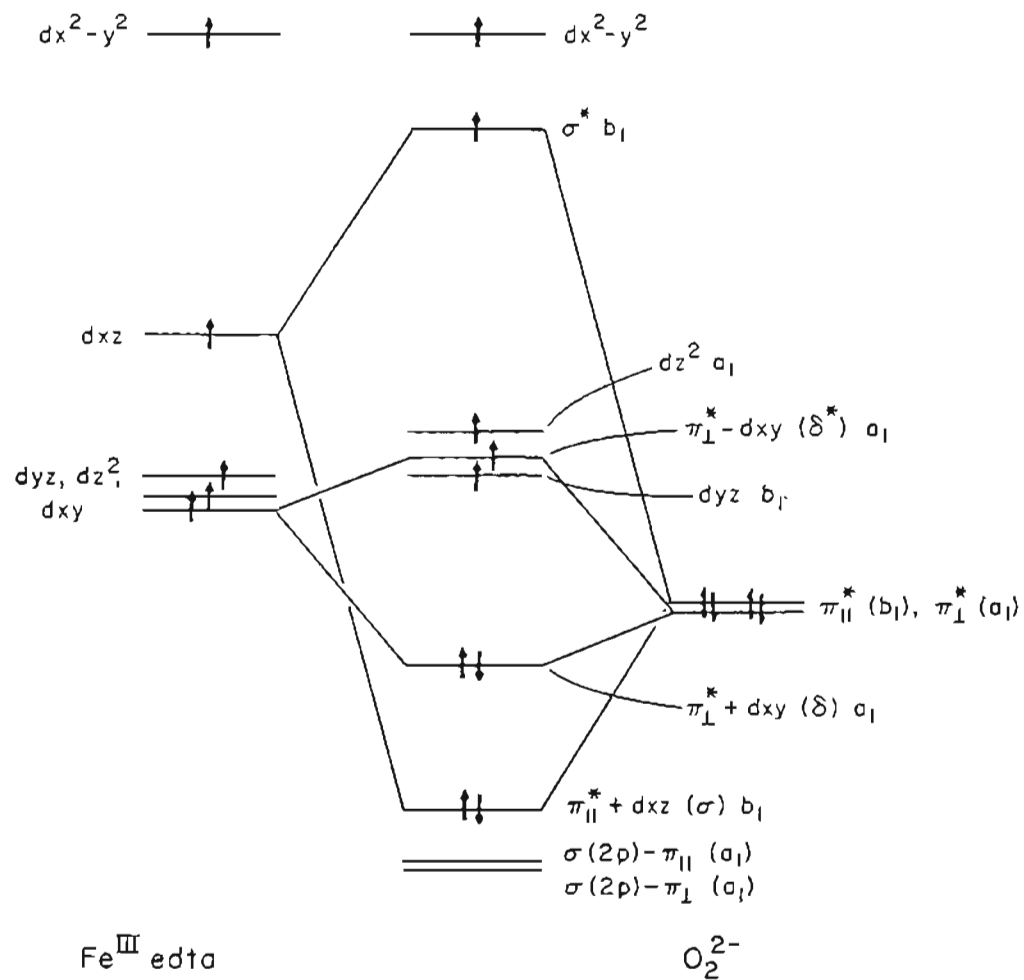
Figure 9. The MO diagram of peroxide bound in an η^2 geometry to Fe^{III}edta with the O–O bond axis parallel to the x-axis of Figure 8. The maximum separation of the iron 3d-orbitals is estimated at -3 eV. See discussion on pages 16-18.

Figure 10. The MO diagram of peroxide bound in an η^2 geometry to Fe^{III}edta with the O–O bond axis parallel to the y-axis of Figure 8. See discussion on pages 16–18.
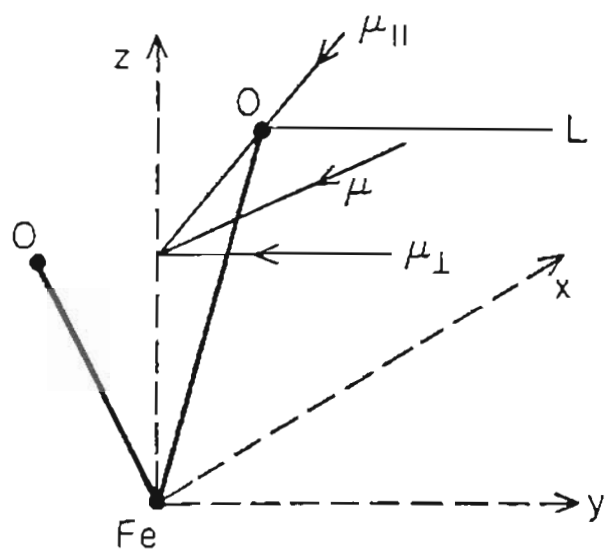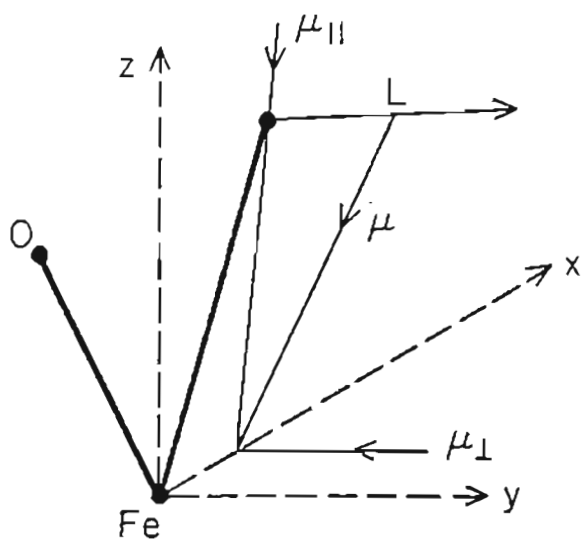
Figure 11. A. Proposed orientation of the electric dipole moment, $\hat{\mu}$, and its || and $\perp$ components for the $\delta(\pi^\star_\perp + d_{xy}) \to d_{z^2}$ transition. See discussion on pages 19 and 20. B. Orientation of $\hat{\mu}$ and its || and $\perp$ components for the $\delta(\pi^\star_\perp + d_{xy}) \to d_{x^2-y^2}$ transition. See page 20.
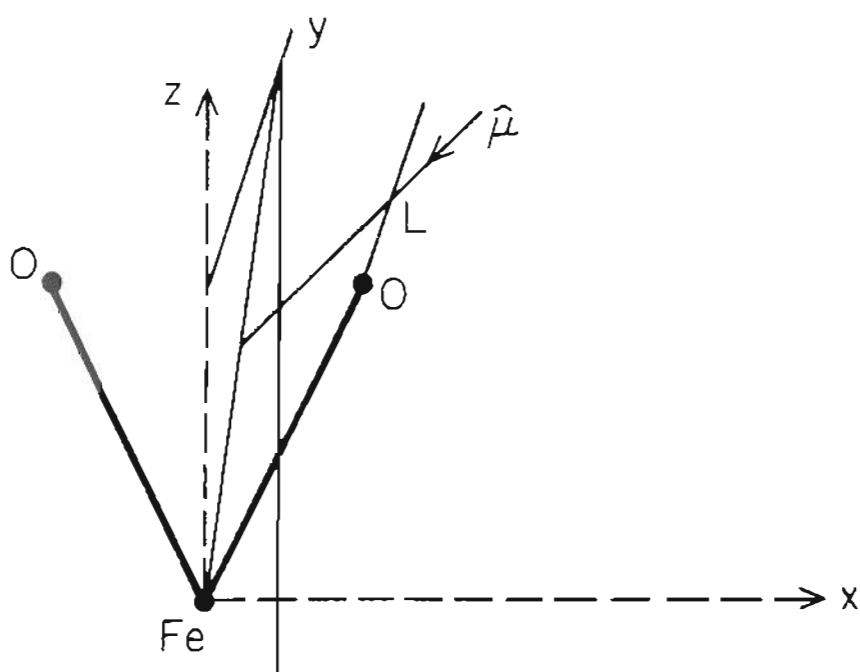
Figure 12. Orientation of $\hat{\mu}$ for the $\delta(\pi^*_\perp + d_{xy}) \rightarrow d_{xy}$ transition that account for the selective enhancement of the O–O vibration over the Fe–O_2 vibration in the resonance Raman spectrum. See discussion on pages 20 and 21.

CHAPTER II

RAMAN SPECTROSCOPIC EVIDENCE FOR SIDE-ON BINDING OF PEROXIDE ION

TO FERRIC-EDTA[1]

Introduction

The bonding of dioxygen to transition metal complexes has been of
interest for some time because of the biological and industrial
importance of oxygen activation by metals.[2] The common modes of
dioxygen binding to metal ions are illustrated in Table II of Chapter
I. In mononuclear superoxo complexes, η^1 (end-on) geometries
predominate, whereas η^2 (side-on) structures are favored for
mononuclear peroxides. In binuclear complexes, $\eta^1:\eta^1$ is the most
common geometry for both peroxo and superoxo species, but $\eta^1:\eta^2$ and
$\eta^2:\eta^2$ coordination have also been observed.[3, 4]

Information on the electronic structure and binding geometry in
metal-dioxygen complexes can be obtained from the O-O stretching
vibration. The frequency of this vibration, $\nu(O-O)$, is indicative of
the O-O bond order,[5] with bands in the $1030-1180-cm^{-1}$ region being
characteristic of superoxides and those in the $750-950-cm^{-1}$ region
being diagnostic of peroxides.[6] The splitting and shift in $\nu(O-O)$ upon
substitution of the bound dioxygen with an asymmetrically labeled
isotope, i.e., $^{16}O^{18}O$, can provide definitive evidence for an η^1 or η^2
type structure.[7] In a mononuclear complex of type η^1, $\nu(^{16}O-^{18}O)$
shifts down in energy relative to $\nu(^{16}O-^{16}O)$ and is split into two
closely spaced bands of equal intensity reflecting the two species

which result from metal coordination to the isotopically distinct

oxygens atoms. In a mononuclear complex of type η^2, $\nu(O-O)$ also shifts

down in energy, but yields only a single vibrational component.

Examples of these two cases are seen for the η^1 ferric peroxide complex

of oxyhemerythrin [$\nu(^{16}O-^{16}O)$ at 845 cm^{-1}; $\nu(^{16}O-^{18}O)$ at 825 and 818

cm^{-1}][8] and for the η^2 matrix isolated complex derived from the reaction

of Fe vapor with O_2 [$\nu(^{16}O-^{16}O)$ at 946 cm^{-1}; $\nu(^{16}O-^{18}O)$ at 931 cm^{-1}].[9]

The purpose of the present study is to determine the mode of

dioxygen binding in the purple complex formed from the reaction of

excess hydrogen peroxide with Fe^{III}-ethylenediaminetetraacetate in

alkaline solution. Previous studies have shown that the stoichiometry

of the formation of the purple complex is 1:1 in Fe(edta) and peroxide,

that the iron is fully paramagnetic high spin Fe(III), and that the

complex is best formulated as $[Fe^{III}(edta)O_2]^{3-}$ or some stoichiometric

equivalent.[10] Although η^2 side-on binding of dioxygen is more likely

for a mononuclear peroxide complex (Table I), and has been suggested as

such by Bull et al.,[11] NMR proton relaxation studies have been

interpreted as favoring an η^1 end-on, protonated structure for the

Fe(edta)-peroxo complex.[12] A resolution of this controversy is of

interest in view of the potential role of ferric(edta) complexes with

hydroperoxides as model systems for nonheme-iron-containing

oxygenases[13] and respiratory proteins such as hemerythrin.[14]

The Fe(edta)-peroxo complex is amenable to study by resonance

Raman spectroscopy, and a vibration at 824 cm^{-1} has been identified as

the O-O stretch of the bound peroxo group.[15] Further vibrational

characterization has now been made possible through the availability of $H_2{}^{16}O{}^{18}O$ prepared as a nearly neat reagent from an $H^{18}OF$ intermediate.[16] Earlier vibrational spectroscopic studies with mixed isotopes of dioxygen were complicated by using a statistical mixture of ${}^{16}O{}^{16}O$, ${}^{16}O{}^{18}O$, and ${}^{18}O{}^{18}O$ species.[8,9] A neat sample of gaseous ${}^{16}O{}^{18}O$ was first used to elucidate the η^1 binding of dioxygen in oxyhemoglobin.[17] In the present study, a similarly neat sample of mixed isotope hydrogen peroxide has enabled us to determine the mode of peroxo coordination to ferric(edta).

Experimental Section

NaFe(edta)·3H$_2$O was prepared by mixing a solution of 250 mM FeCl$_3$·6H$_2$O with a three-fold excess of NaOH and an equimolar amount of Na$_2$H$_2$(edta), heating for 10 min at 80-90°, and slow evaporation to yield yellow-brown crystals.[18] The peroxo complex, $[Fe(edta)O_2]^{3-}$, was prepared by dissolving NaFe(edta)·3H$_2$O in 1 M Na$_2$CO$_3$ followed by the addition of 30% H$_2$O$_2$ (Sigma) to give a solution 50 mM in Fe and 150-200 mM in peroxide with a pH between 9.5 and 10.5. The resulting purple solution had the expected absorption maximum at 520 nm[10] and was stable for about 1 hr at 4°C. $[Fe(edta)O_2]^{3-}$ was also prepared in deuterated solvent by dissolving NaFe(edta)·3H$_2$O in 1 M Na$_2$CO$_3$ in D$_2$O (Aldrich 99.8 atom-% D) followed by the addition of 30% H$_2$O$_2$ in H$_2$O. The isotopic composition of the final solution was 97% deuterium and 3% hydrogen.

Isotopically labelled hypofluorous acid, $H^{18}OF$, was prepared by

reacting F_2 with $H_2{}^{18}O$ ice (Norsk Hydro, 99+ atom-% ^{18}O) as described previously.[16] The labelled $H^{18}OF$ was then transferred into $H_2{}^{16}O$ water yielding a solution 0.3 M in $H_2{}^{16}O^{18}O$ and 0.5 M in HF, which was frozen to minimize further decomposition. This material was later reacted with NaFe(edta)·$3H_2O$ as described above to produce the mixed isotope peroxide complex. The 1 M Na_2CO_3 was adequate to neutralize the HF and maintain the final solution above pH 9 in the region of maximal stability for the peroxo complex.[12]

Resonance Raman spectra were recorded on a computer-interfaced Jarrell- Ash spectrophotometer[19] equipped with a Spectra-Physics 164-05 (Ar) ion laser, a Spectra-Physics 2025-11 Kr ion laser, an RCA C31034A photomultiplier tube, and an ORTEC Model 9302 amplifier/discriminator. Samples studied at 15 K were directly frozen onto a gold-plated copper cold finger in a closed-cycle helium Displex (Air Products). Samples at 90 K were frozen either directly on an aluminum sample holder attached to a cold finger or inside a glass capillary inserted into a copper cold finger[20] which was immersed in a Dewar cooled with liquid N_2. The integrity of samples at ~278 K was maintained by flowing the solutions in capillary tubing through a chilled bath.[21] Data from frozen samples were collected in a 150° backscattering geometry, whereas 90° scattering was used on cooled solution samples. Isotope comparisons were carried out on spectra collected under identical conditions and acquired in sequential order. Reported peak frequencies are accurate to ± 0.5 cm^{-1}.

Results

In the previously reported resonance Raman spectrum of $[Fe(edta)O_2]^{3-}$, peaks were observed at 472 and 824 cm^{-1} using a spinning sample at room temperature.[15] The 824-cm^{-1} band was assigned as the O-O stretch of a bound peroxide on the basis of its frequency and its enhancement profile tracking the 520-nm $O_2^{2-} \rightarrow Fe^{III}$ charge transfer band.[15] Lowering the temperature to 90 K gives increased sample stability and a shift in $\nu(O-O)$ to 815 cm^{-1} (Figure 1). Although the purple solution gains an orange tinge upon freezing, the enhancement maximum for $\nu(O-O)$ remains at ~520 nm. The color change most likely arises from a sharpened electronic absorption band with diminished intensity in the long-wavelength shoulder. The broad feature at ~470 cm^{-1} is still noted for samples frozen in glass capillaries, but it is markedly diminished in samples frozen directly onto cold fingers at either 90 K or 15 K where the glass windows of the chamber are considerably farther removed from the scattering surface. Since glass alone displays a broad band centered at ~470 cm^{-1}, it seems likely that this spectral feature arises mainly from the glass capillary and is only prominent in the spectrum of the $[Fe(edta)O_2]^{3-}$ because $\nu(O-O)$ is rather weakly resonance enhanced.

When mixed isotope hydrogen peroxide is used to form the $Fe^{III}(edta)$-peroxo complex, the O-O stretch at 815 cm^{-1} shifts cleanly to 794 cm^{-1} with no detectable splitting (Figure 1). The single peak is diagnostic of an η^2 configuration in which the two oxygens are equivalent.[7] A simple Hooke's law calculation gives a value of 23 cm^{-1}

for the expected downshift in ν(O–O) upon isotopic substitution with $^{16}O^{18}O$, which agrees well with the experimental value of 21 cm^{-1}.

The alternative proposed structure for the Fe^{III}(edta)-peroxo complex has the dioxygen coordinated as an end-on bound hydroperoxide.[12] In this structure, ν(O–O) would be expected to exhibit a deuterium isotope effect. The spectra of $[Fe(edta)O_2]^{3-}$ in H_2O and D_2O obtained at 15 K are shown in Figure 2. There is no detectable shift of the 815-cm^{-1} ν(O–O) in the D_2O sample. The small feature at 877 cm^{-1} is due to ν(O–O) of unreacted H_2O_2. A similar lack of a deuterium isotope effect was observed for samples at 5°C. Thus, the bound dioxygen shows no indication of either protonation or hydrogen bonding in the Fe^{III}(edta)-peroxo complex.

A control experiment was performed on hydrogen peroxide to quantitate the deuterium sensitivity of ν(O–O) in a species known to be protonated at neutral pH. Previous studies of the vibrational spectrum of H_2O_2 reported ν(O–O) at 878-880 cm^{-1} with little or no shift in deuterium.[22, 23] Figure 3 shows Raman spectra of 1 M solutions of hydrogen peroxide in H_2O and D_2O obtained at 15 K. The high resolution achieved with low temperature samples makes it clear that the O–O stretch occurs at 877 cm^{-1} in H_2O and shifts up to 879 cm^{-1} in D_2O.

The Raman spectrum of hydrogen peroxide in the frozen state is complicated by the appearance of shoulders at higher and lower energy relative to the principal O–O vibration. The intensities of these minor components were found to vary with sample temperature and rate of freezing. They were not observed in liquid samples and were

considerably diminished by the addition of 1% glycerol prior to freezing. Since glycerol alters the structure of the frozen solvent, it is likely that the appearance of multiple O–O vibrations is related to hydrogen-bonding properties of the solvent in the frozen state. The frequency of the major Raman peak and its 2-cm^{-1} shift to higher energy in D_2O was unaffected by the addition of glycerol. In liquid samples at room temperature, the O–O stretching mode was observed at 875 cm^{-1} in H_2O_2 and at 876 cm^{-1} in D_2O_2.

The shift of the hydrogen peroxide ν(O–O) to higher energy in D_2O is anomalous in view of the expected decrease in frequency with increasing mass. The upward shift most likely relates to the hydrogen-bonding interactions between the peroxide oxygens and solvent protons. If deuterium forms a weaker hydrogen bond than hydrogen, this causes a relatively greater bonding electron density to remain in the O–O bond, thereby accounting for the increase in frequency. Such deuterium-dependent upshifts in hydrogen-bonded moieties have been observed for the Fe–O–Fe symmetric stretch in oxyhemerythrin and the C–O–C asymmetric stretch in 2-methoxyethanol.[24] Alternatively, since deuterium tends to form stronger σ bonds than hydrogen, the O–O bond of D_2O_2 or DO_2^- could be strengthened if the σ bonding involved significant withdrawal of electron density from the filled antibonding π^* orbitals on the oxygen atoms. The latter explanation has been invoked for the deuterium-dependent upshift in ν(O–O) of the iron-bound peroxide in oxyhemerythrin.[21, 25]

Discussion

The observation of $\nu(O-O)$ for the Fe(edta)-peroxo complex at 824 cm^{-1} in solution and at 815 cm^{-1} in the frozen state establishes that the bound dioxygen species is a peroxide. Similar peroxide vibrations have been reported at 766 cm^{-1} in Na_2O_2 and at 806 cm^{-1} in the $Fe^{III}OEP$-peroxo complex.[26, 27] The η^2 side-on binding of peroxide in the $[Fe(edta)O_2]^{3-}$ complex is conclusively demonstrated by our isotope substitution experiments. Other established examples of side-on binding of dioxygen include $[Mn^{III}TPP(O_2)]^-$ and $[V^VO(IDA)-(O_2)]^-$ whose structures have been verified by X-ray crystallography and whose O-O vibrations are at 983 and 920 cm^{-1}, respectively.[28, 29] Infrared and EXAFS data on $[Fe^{III}TPP(O_2)]^-$ and $[Ti^{IV}TPP(O_2)]^-$ indicate that the bound dioxygen is also in a side-on peroxo configuration.[27, 30] Furthermore, the η^2 structure has been proposed as an intermediate in the oxidation of $Fe^{II}(edta)$ by H_2O_2,[31] and the present results with $Fe^{III}(edta)$ make this a likely probability.

The structures of the reactive forms of $Fe^{III}(edta)$ and hydrogen peroxide as well as the resultant peroxo complex have been the subject of much conjecture. In the crystal structure of $[Fe(edta)OH_2]^-$ reported by Lind et al.,[32] the seven-coordinate iron has a distorted pentagonal bipyramidal geometry. The two amine nitrogens, two monodentate carboxylate oxygens (one from each N-), and the water molecule occupy the pentagonal plane, whereas the remaining two carboxylates coordinate to the axial positions. Nucleophilic ligands seem to be capable of displacing the water molecule to form

$[Fe^{III}(edta)L]^{2-}$ complexes.[33] If a similar structure formed with peroxide, it would have the configuration shown in Figure 4a. Alternatively, the side-on binding of peroxide could be accompanied by the displacement of both the water and a carboxylate ligand, resulting in a more nearly octahedral geometry (Figure 4b).

There is reasonably good agreement that the predominant solution species between pH 8.0 and 10.0 is $[Fe^{III}(edta)(OH)]^{2-}$, which then reacts with either H_2O_2 or HO_2^- to produce the peroxo complex.[11, 12] The $[Fe^{III}(edta)OH]^{2-}$ species is likely to have a seven-coordinate geometry similar to that of its protonated analog, $[Fe^{III}(edta)OH_2]^-$. The overall reaction can be written as:

$$[Fe^{III}(edta)OH]^{2-} + H_2O_2 \; \underset{\leftarrow}{\rightarrow} \; [Fe^{III}(edta)O_2]^{3-} + H_3O^+ \quad (1)$$
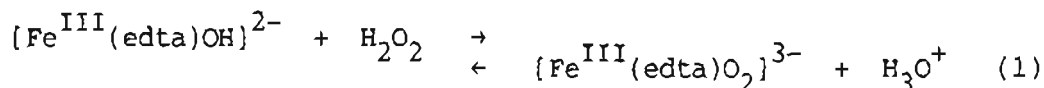
According to Bull et al.,[11] reaction (1) proceeds via the initial dissociation of hydroxide, followed by the formation of the peroxide adduct and the concomitant release of protons. The sensitivity of the forward reaction to general acid/base catalysis is explained as H^+-assistance of hydroxide dissociation and general-base assistance of peroxide deprotonation. The second order rate constant in the absence of general acid catalysis is $\sim 3 \times 10^2$ $M^{-1} s^{-1}$.[11, 34] Interestingly, the reaction

$$[Fe^{II}(edta)]^{2-} + O_2^{\cdot-} \; \underset{\leftarrow}{\rightarrow} \; [Fe^{III}(edta)O_2]^{3-} \quad (2)$$
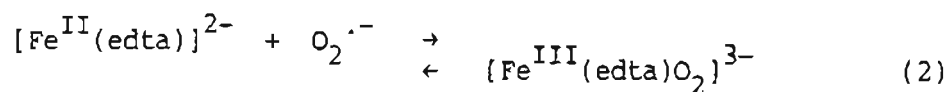
forms the identical product by oxidative addition without the apparent
need for hydroxide or proton dissociation and proceeds -2×10^4-fold
faster.[11] Although it has been proposed on the basis of water proton
relaxation rates that the OH$^-$ ligand is still present in the peroxo
complex and that it is an edta carboxyl group which is displaced,[12]
hydroxide displacement seems more likely to account for the difference
in peroxide and superoxide reaction rates as well as for the observed
single proton dependence of the back reaction.[11] Thus, the species in
Figure 4a is the more probable structure for the Fe^{III}(edta)-peroxo
complex.

Since the η^2 configuration is the generally observed mode of
dioxygen binding in mononuclear metal-peroxo complexes, the protein
oxyhemerythrin appears to represent an exception. The combination of
X-ray crystallographic[35] and resonance Raman[8, 36] results makes it
certain that the dioxygen is reduced to peroxide and is coordinated to
a single Fe(III) in an η^1 end-on fashion. The O—O stretch at 844 cm^{-1}
in oxyhemerythrin shifts 4 cm^{-1} to higher energy in D$_2$O, implying that
the bound peroxide is protonated.[21] The end-on binding of
hydroperoxide appears to be enforced by steric restrictions at the
oxygen binding site and by the presence of an Fe—O—Fe moiety (a
suitable hydrogen bond acceptor) which anchors the hydroperoxide ion in
place.[24, 35] These conditions allow the protein to override the
preferred η^2 orientation of metal-coordinated peroxides.

REFERENCES

(1)   Ahmad, S.; McCallum, J. D.; Shiemke, A. K.; Appelman, E. H.;
      Loehr, T. M.; Sanders-Loehr, J. Inorg. Chem. 1988, 27, 2230.

(2)   (a) Molecular Mechanisms of Oxygen Activation; Hayaishi, O.,
      Ed.; Academic: New York, 1974; (b) Oxidases and Related Redox
      Systems; King, T. E.; Mason, H. S.; Morrison, M., Eds.;
      Pergamon: Oxford, 1982; (c) Oxygen Complexes and Oxygen
      Activation by Metal Complexes; Martell, A. E., Ed.; Plenum: New
      York, 1988, in press.

(3)   Gubelmann, M. H.; Williams, A. F. Struct. Bonding (Berlin)
      1983, 55, 1.

(4)   (a) Lever, A. B. P.; Gray, H. B. Acc. Chem. Res. 1978, 11, 348;
      (b) Valentine, J. S.; McCandlish, E. In Electron Transport and
      Oxygen Utilization; Ho, C., Ed.; Elsevier North-Holland:
      Amsterdam, 1982; p 229.

(5)   Herzberg, G. Molecular Spectra and Molecular Structure; Van
      Nostrand: New York, 1950.

(6)   Suzuki, M.; Ishiguro, T.; Kozuka, M.; Nakamoto, K. Inorg. Chem.
      1981, 20, 1993.

(7)   (a) Huber, H.; Klotzbucher W.; Ozin, G. A.; Van der Voet, A.
      Can. J. Chem. 1973, 51, 2722. (b) Loehr, T. M. In Oxygen
      Complexes and Oxygen Activation by Metal Complexes; Martell, A.
      E., Ed.; Plenum: New York, 1988, in press.

(8)   Kurtz, D. M., Jr.; Shriver, D. F.; Klotz, I. M. J. Am. Chem.
      Soc. 1976, 98, 5033.

(9)   Abramowitz, S.; Acquista, N.; Levin, I. W. Chem. Phys. Lett.

1977, <u>50</u>, 423.

(10) Walling, C.; Kurz, M.; Schugar, H. J. <u>Inorg. Chem.</u> 1970, <u>9</u>, 931.

(11) Bull, C.; McClune, G. J.; Fee, J. A. <u>J. Am. Chem. Soc.</u> 1983, <u>105</u>, 5290.

(12) Francis, K. C.; Cummins, D.; Oakes J. <u>J. Chem. Soc. Dalton Trans.</u> 1985, 493.

(13) Balasubramanian, P. N.; Bruice, T. C. <u>Proc. Natl. Acad. Sci. U. S. A.</u> 1987, <u>84</u>, 1734.

(14) Wilkins, P. C.; Wilkins, R. G. <u>Coord. Chem. Rev.</u> 1987, <u>79</u>, 195.

(15) Hester, R. E.; Nour, E. M. <u>J. Raman Spectrosc.</u> 1981, <u>11</u>, 35.

(16) Appelman, E. H.; Jache, A. W. <u>J. Am. Chem. Soc.</u> 1987, <u>109</u>, 1754.

(17) Duff, L. L.; Appelman, E. H.; Shriver, D. F.; Klotz, I. M.; <u>Biochem. Biophys. Res. Commun.</u> 1979, <u>90</u>, 1098.

(18) Schugar, H. J.; Hubbard, A. T.; Anson, F. C.; Gray, H. B. <u>J. Am. Chem. Soc.</u> 1969, <u>91</u>, 71.

(19) Loehr, T. M.; Keyes, W. E.; Pincus, P. A. <u>Anal. Biochem.</u> 1979, <u>96</u>, 456.

(20) Sjöberg, B. M.; Loehr, T. M.; Sanders-Loehr, J. <u>Biochemistry</u> 1982, <u>21</u>, 96.

(21) Shiemke, A. K.; Loehr, T. M.; Sanders-Loehr, J. <u>J. Am. Chem. Soc.</u> 1984, <u>106</u>, 4951.

(22) Bain, O.; Giguère, P. A. <u>Can. J. Chem.</u> 1955, <u>33</u>, 527.

(23) Taylor, R. C.; Cross, P. C. <u>J. Chem. Phys.</u> 1956, <u>24</u>, 41.

(24) Shiemke, A. K.; Loehr, T. M.; Sanders-Loehr, J. <u>J. Am. Chem. Soc.</u> 1986, <u>108</u>, 2437.

(25) Kurtz, D. M., Jr., Ph.D. Dissertation, Northwestern University,

1977.

(26) Evans, J. C. J. Chem. Soc. Dalton Trans. 1969, 682.

(27) McCandlish, E.; Miksztal, A. R.; Nappa, M.; Sprenger, A. Q.; Valentine, J. S.; Stong, J. D.; Spiro, T. G. J. Am. Chem. Soc. 1980, 102, 4268.

(28) VanAtta, R. B.; Strouse, C. E.; Hanson, L. K.; Valentine, J. S. J. Am. Chem. Soc. 1987, 109, 1425.

(29) Djordjevic, C.; Craig, S. A.; Sinn, E. Inorg. Chem. 1985, 24, 1283.

(30) Friant, P.; Goulon, J.; Fischer, J.; Ricard, L.; Schappacher, M.; Weiss, R.; Momenteau, M. Nouv. J. Chim. 1985, 9, 33.

(31) Rush, J. D.; Koppenol, W. H. J. Inorg. Biochem. 1987, 29, 199.

(32) Lind, M. D.; Hamor, M. J.; Hamor, T. A.; Hoard, J. L. Inorg. Chem. 1964, 3, 34.

(33) Phillip, C. V.; Brooks, D. W. Inorg. Chem. 1974, 13, 384.

(34) Orhanović, M.; Wilkins, R. G. Croat. Chim. Acta. 1967, 39, 149.

(35) Stenkamp, R. E.; Sieker, L. C.; Jensen, L. H.; McCallum, J. D.; Sanders-Loehr, J. Proc. Natl. Acad. Sci. U. S. A. 1985, 82, 713.

(36) Dunn, J. B. R.; Shriver, D. F.; Klotz, I. M. Proc. Natl. Acad. Sci. U. S. A. 1973, 70, 2582.

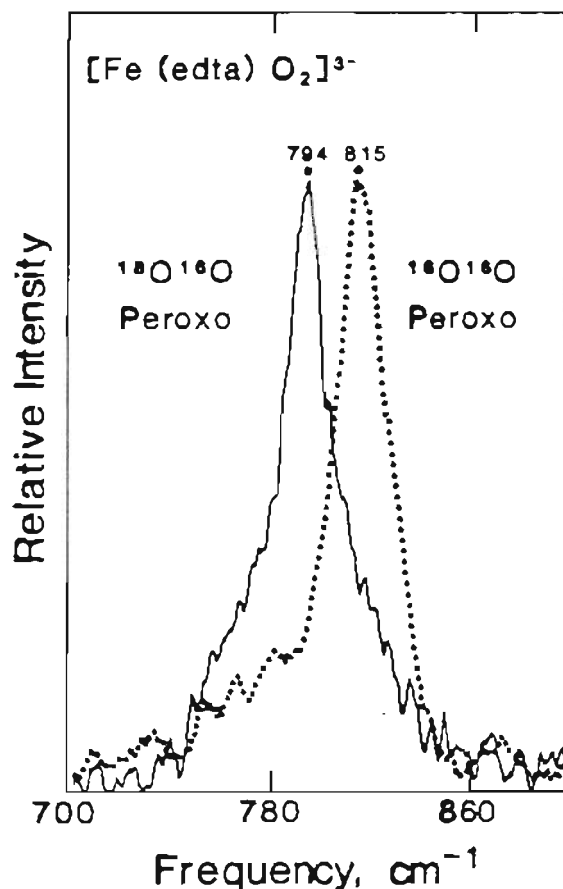Figure 1. Resonance Raman spectrum of $[Fe(edta)O_2]^{3-}$ prepared from $H_2^{18}O^{16}O$ (_____) or $H_2^{16}O^{16}O$ (- - -). Samples contained 50 mM Fe and a 3-fold excess of H_2O_2. Spectra were obtained from samples in capillaries at 90 K with 514.5-nm excitation (100 mW at the sample) and a slit width of 5 cm^{-1}. A total of 10 scans of the $^{16}O^{16}O$-containing sample were collected at 1 cm^{-1}/s and subjected to a 25-point smooth. Data for the $^{16}O^{18}O$-containing sample were collected at 0.5 cm^{-1}/s, 18 scans, and given a 25-point smooth.
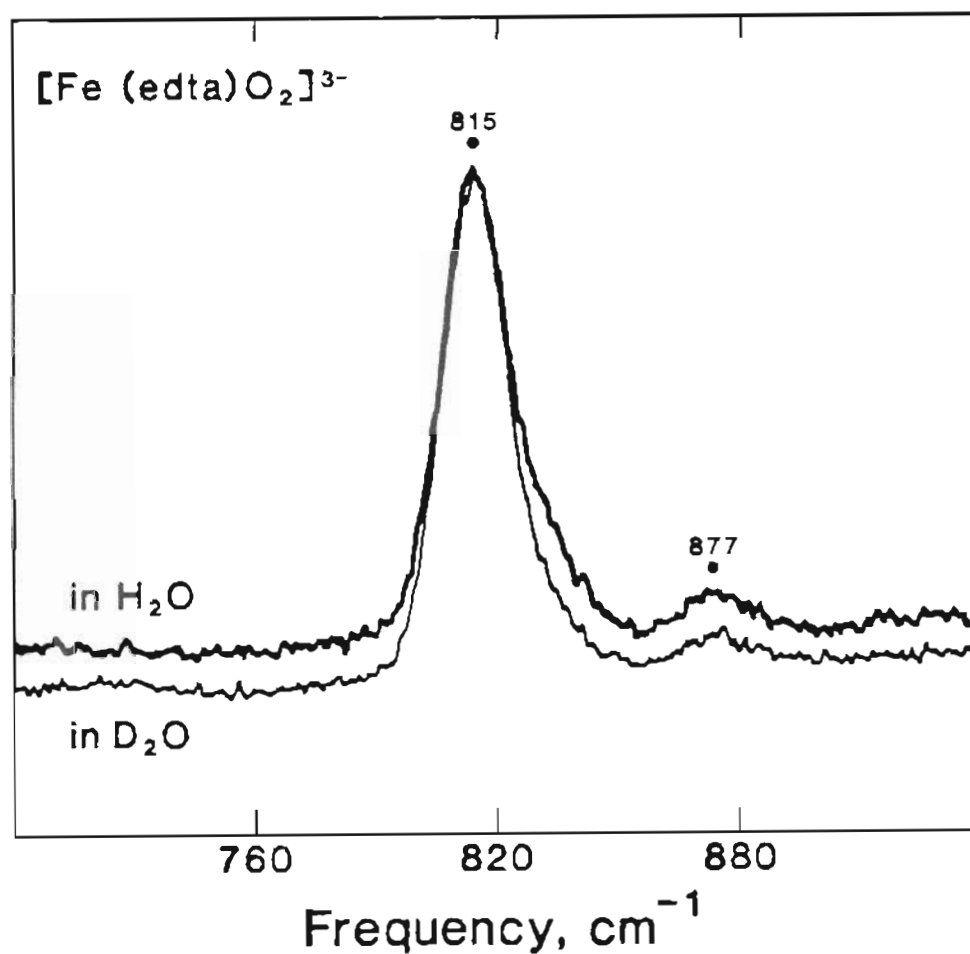
Figure 2. Resonance Raman spectrum of $[Fe(edta)O_2]^{3-}$ in H_2O and in D_2O. Samples (50 mM in Fe) were prepared using a four-fold excess of H_2O_2. Spectra were obtained at 15 K with 514.5-nm excitation (60 mW at the sample) and a slit width of 5 cm^{-1}. Six scans were collected at 0.5 cm^{-1}/s followed by a 13-point smooth.
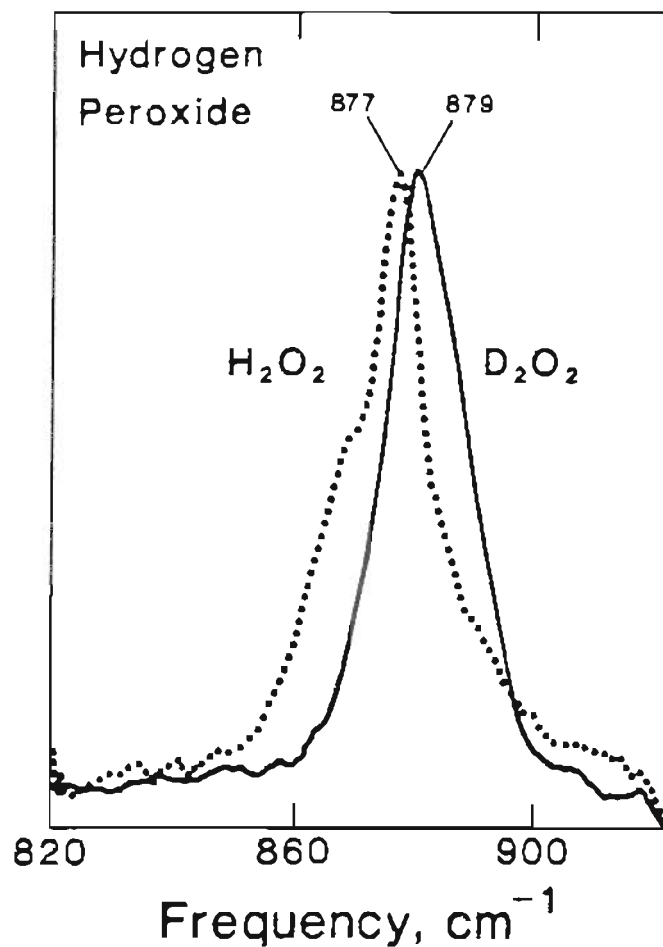
Figure 3. Raman spectrum of hydrogen peroxide (1.5 M) in H_2O and D_2O. Samples were prepared by mixing 170 μL of a 30% solution (aq) of H_2O_2, 10 μL of glycerol and 820 μL of H_2O or D_2O to give a total volume of 1 mL. Spectra were obtained at 15 K with 647.1-nm excitation (60 mW at the sample) and a slit width of 5 cm^{-1}. The data were collected at 0.5 cm^{-1}/s and were given a 17-point smooth. The greater peak width for the major component in D_2O is most likely due to the presence of ~18% hydrogen in this sample.
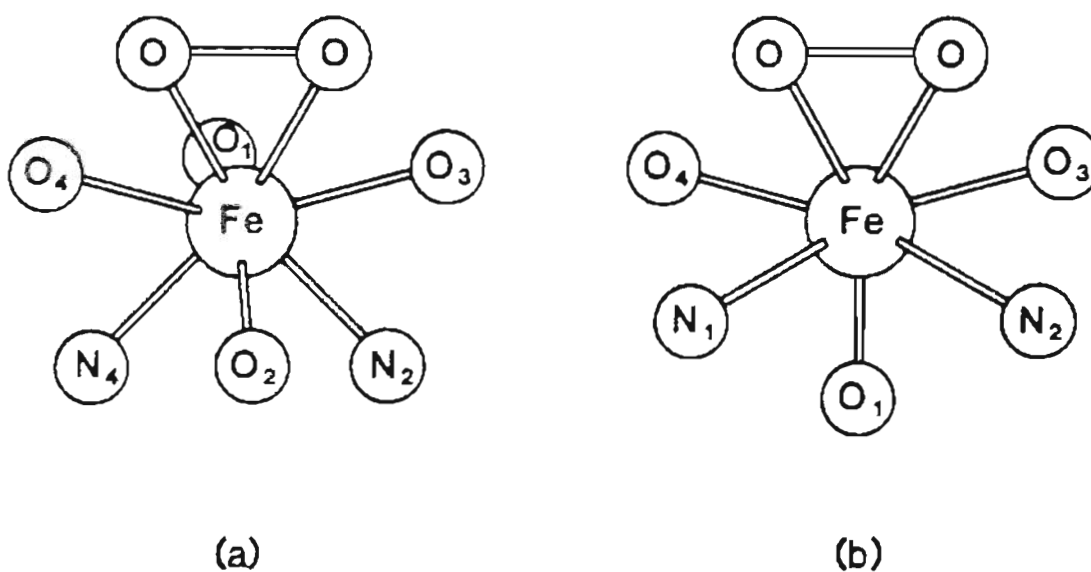
(a)

(b)

Figure 4. Possible structures of $[Fe^{III}(edta)O_2]^{3-}$. (a) Derived from the peroxide displacement of the water in the seven-coordinate $[Fe^{III}(edta)(OH_2)]^-$ complex. N_1, N_2, and O_1-O_4 are edta ligands with atom positions similar to those in $[Fe^{III}(edta)OH_2]^{3-}$.[32] (b) Derived from the displacement of a carboxylate oxygen as well as the water molecule.

BIOGRAPHICAL SKETCH

The author was born in Chittagong, Bangladesh, on January 30, 1962. He later moved with his family to Lahore, Pakistan, where he obtained his basic schooling. In 1980, he was awarded a Reed Women's Committee Scholarship which enabled him to pursue an undergraduate education at Reed College in Portland, Oregon. In addition to academic interests in chemistry, physics, mathematics, and writing, the author was also an active member of the Reed College squash and soccer teams. He graduated from Reed in May, 1985, with a B.A. in Chemistry.

He began graduate studies at Oregon Graduate Center in August, 1985. In his research at OGC, the author has contributed to a number of different projects related to the O_2 transport protein, hemerythrin. Initially, he developed a procedure for the anaerobic crystallization of deoxyhemerythrin, which was later adopted in an X-ray structure determination. He performed Raman spectroscopic studies to determine the relationship between the absorption spectrum and the excitation profile of the Fe-O-Fe vibration in the protein. He also carried out kinetic studies to determine the rate of exchange of the Fe-O-Fe oxygen with solvent in deoxyhemerythrin. Finally, he investigated the structure of the peroxide complex of ferric-ethylenediaminetetraacetate as a model for the O_2 complex of oxyhemerythrin. This latter study has been published, and serves as the basis for this M. S. dissertation. Publication:

Salman Ahmad, John D. McCallum, Andrew K. Shiemke, Evan H. Appelman, Thomas M. Loehr, and Joann Sanders-Loehr (1988) Inorganic Chemistry 27, 2230-2233.